REVISION 1

A new framework topology in the dehydrated form of zeolite levyne

R. Arletti[1], G. Vezzalini[2] , S. Quartieri[3], F. Cámara[1], M. Alvaro[4]

[1] Dipartimento di Scienze della Terra, Università di Torino

[2] Dipartimento di Scienze Chimiche e Geologiche, Università di Modena e Reggio Emilia

[3] Dipartimento di Fisica e Scienze della Terra, Università di Messina

[4] Dipartimento di Scienze della Terra e dell'Ambiente, Università degli Studi di Pavia, Italy,
Int'l Research School of Planetary Sciences, Università G. d'Annunzio, Chieti, Italy

ABSTRACT

The thermoelastic behavior and structural evolution of a natural levyne-Ca [$(Ca_{7.8}Na_{2.2}K_{1.1})_{\Sigma 11.1}Al_{20.0}Si_{34.2}O_{108}\cdot 51.5H_2O$; S.G. $R\bar{3}m$; a = 13.377(4) Å, c = 22.870(1) Å, V = 3544.1(3) Å^3] were studied by both T-resolved synchrotron X-ray powder diffraction (SR-XRPD) between room-temperature and 800 °C, and by conventional-source high-temperature single crystal X-ray diffraction (SC-XRD). Above 230°C, water loss and reallocation of extraframework cations induce the strain and consequent breaking of T-O-T bridges in the D6R, with resulting migration of tetrahedral cations to new tetrahedral sites. The new tetrahedra virtually share an edge with the previously occupied tetrahedra. This phenomenon gives rise to a new topology which coexists, in a percentage of about 40%, with the original one. The new framework consists of a sequence of a novel zeolitic cage (described as a 20-hedron formed by fourteen 6mR and six 4mR) and two consecutive cancrinite cages along [0001]. This topology – reported in the database of the hypothetical zeolite structures as 166_2_293 – belongs to the ABC-6 family and can be described by the following sequence of 6-rings: **ABCBCACAB**, to be compared with that of levyne AABCCABBC. In the new topology the extraframework cations are distributed over 3 new sites: one at the center of the 6mR ⊥ [0001] shared by the two cancrinite cages, one near the center of the 6mR ⊥ [0001] at the base of the new cage, and a last one in a 6mR window of the new cage. The

8mR bidimensional channel system originally present in levyne is therefore absent in the new topology and hence molecular diffusion is likely to be partially hindered in the dehydrated form. The phase transition is not completely reversible, at least in the short term, as only partial rehydration was demonstrated.

INTRODUCTION

Zeolite dehydration mechanisms have been widely studied because the sorptive and catalytic properties of these materials are profoundly influenced by the dehydration and calcination processes, which occur at relatively high temperature (H*T*). The knowledge of the structural modifications induced by temperature and the definition of the stability field of these materials is of prime importance to assure their persistence and effectiveness in technological applications.

The behavior of zeolites upon heating, and the definition of the factors governing their stability, have been described by several authors (Alberti and Vezzalini 1984; Bish and Carey 2001; Alberti and Martucci 2005; Cruciani 2006,). Alberti and Vezzalini (1984) classified the structural changes induced by the heating of zeolites into three categories – the same classification was also adopted by Bish and Carey (2001): i) reversible dehydration accompanied by rearrangement of the cations without significant changes in the framework and cell volume; ii) complete or nearly complete reversible dehydration accompanied by a strong distortion of the framework and a large decrease in cell volume; iii): dehydration accompanied by topological changes in the framework.

In general, the changes occurring in this latter category are due to the breaking of T-O-T bridges and the migration of the tetrahedral cations to new tetrahedral sites. The new tetrahedra are called *face sharing tetrahedra* (Alberti and Vezzalini 1984; Alberti and Martucci 2011) and have three vertices as before, with a new fourth apex occupied by H_2O or (OH) groups. These bridging interruptions are induced by the strains of extraframework cations – initially located in the channels and solvated – migrated closer to the framework oxygen atoms in order to achieve a more suitable coordination after water release.

This process is mainly exhibited by zeolites with frameworks formed from chains of $4^2 5^4$ Secondary Building Units (SBUs): stilbite (Galli and Gottardi 1966; Slaughter 1970; Mortier 1983; Cruciani et al. 1997), barrerite (Galli and Alberti 1976; Alberti and Vezzalini 1978; Alberti et al. 1983), stellerite (Galli and Alberti 1975; Alberti et al. 1978), heulandite (Merkle and Slaughter 1968; Alberti 1972; Alberti 1973; Alberti and Vezzalini 1983; Alberti et al. 1985), clinoptilolite (Armbruster and Gunter 1991; Armbruster 1993), and brewsterite (Alberti et al. 1999; Ståhl and Hanson 1999; Sacerdoti et al. 2000; Alberti et al. 2001).

As observed by Arletti et al. (2006) and also reported by Cruciani (2006), external factors strictly control the thermal behavior of zeolites. A good example to typify the structural differences observed under different experimental conditions is the recent time-resolved study of stellerite (Arletti et al. 2006), performed by 'in situ' X-ray Powder Diffraction (XRPD), compared to the previous study performed 'ex situ' on single crystals dehydrated under vacuum at selected temperatures and measured in ambient conditions (Alberti et al. 1978). The results of the 'in situ' study confirmed the breaking of a T–O–T bridge in the four-ring of the $4^2 5^4$ cage but on a different bridge with respect to that found in stellerite in the 'ex situ' study. Interestingly, in the 'in situ' experiment on stellerite, the same T–O–T bridge was broken as the one previously reported in stilbite studied using a similar technique (Cruciani et al. 1997). The discrepancy between the results from these different heating methods and XRD techniques has also been observed for brewsterite, when a single crystal study reported occurrence of T–O–T bridge breaking (Alberti et al. 1999) which was not found in an 'in situ' XRPD study (Ståhl and Hanson 1999). In wairakite, studied by stepwise heating 'in situ' of single crystal XRD, recovery of the tetragonal topochemical symmetry was reported at 145 °C (Seryotkin et al. 2003), whereas an 'in situ' XRPD study showed that the monoclinic real symmetry was preserved through the entire temperature range (Cruciani and Zanella 2002). **The same phase sharing tetrahedra phenomenon is observed also in synthetic ABW (Norby 1990) and goosecreekite (Wadoski et al. 2010).**

Zeolites that undergo T–O–T bridge breaking include also phases built up of stacking sequences of six rings as the synthetic (Na, TMA)-form of the zeolite EAB (Meier and Groner 1981), the Li-Losod (Sieber and Meier 1974) the sodium form of chabasite (Cartlidge and Meier 1984) and gmelinite (Alberti et al. 2010). All these phases at high temperature convert into different topologies, in particular EAB and sodium form of chabasite transform in sodalite like materials, the Li-Losod transforms into Li-cancrinite, while gmelinite transforms in AFI topology.

The porous materials with levyne topology (LEV) are represented by the natural zeolite levyne (Brewster 1825; Barrer and Kerr 1959) and several synthetic phases including the aluminophosphate AlPO-35 (Zhu et al. 1997), the silicoaluminophosphate SAPO-35 (Lok et al. 1984), the metal aluminophosphate MeAPO-35 (with Me = Fe, Ti, Co, Mg, Mn and Zn), and the metal silicoaluminophosphate ElAPSO-35 (with El = As, B and Ge) systems (Flaningen et al. 1986). Moreover, boron-substituted levynes were first synthesized by Millini et al. (1992).

Notwithstanding a widespread interest in porous materials with levyne topology, their thermal behavior and stability have not been studied in detail until now. The studies performed to date involve thermal analyses of natural levynes (Gottardi and Galli 1985), the structural characterization of a LEV-type aluminosilicate (called RUB-50) in its as-synthesized, calcined and rehydrated calcined forms (Yamamoto et al. 2010), and the thermal stability of boron substituted levynes (Leardini et al. 2013).

In the present work, the thermally induced structural modifications of a natural levyne-Ca were studied both in temperature-resolved synchrotron X-ray powder diffraction (SR-XRPD), and conventional-source high-temperature single crystal X-ray diffraction (SC-XRD) experiments.

Chemical and structural data of levyne

Levyne is an uncommon zeolite with general composition $(Na,K\ Ca_{0.5})_6\ [Al_6Si_{12}O_{36}] \bullet{\sim}17\ H_2O$. The extra-framework cation content ranges from strongly Ca-dominant to strongly Na-dominant, with minor K and, in some cases, minor Sr or Ba. Si:Al is also variable (Galli et al. 1981). Levyne is typically found as a hydrothermal mineral in vugs of massive volcanic rocks.

Merlino et al. (1975) solved its structure in the s.g. $R\bar{3}m$, on the basis of the model previously proposed by Barrer and Kerr (1959). Levyne framework is built up from alternating double (D6R) and single 6-membered rings (6mR) of tetrahedra along [0001], following the stacking sequence AABCCABBC of single tetrahedral layers. The resulting framework is characterized by a tridimensional channel system, perpendicular to the threefold axis, confined by 8-membered rings (8mR) (Figure 1). Along [0001], between two D6R there are two ‘‘levyne cages’’ $[4^9 6^5 8^3]$, sharing a 6mR ⊥ (0001), which host non-framework cations and water molecules. The unit cell contains two crystallographically independent tetrahedral sites, labeled T1 and T2. Single-crystal structural refinements carried out by Sacerdoti (1996) and Gatta et al. (2005) demonstrated that there is only a partial indication of tetrahedral Si–Al ordering. In all these structural refinements of levyne the cation sites are placed along the three-fold symmetry axis inside the levyne cage, and the water sites near the wall of the levyne cage. C1 site is off the plane, but very close to the 6mR ⊥ (0001) window of the D6R and is coordinated to oxygen atoms and water molecules; C2, C3 and C4, at different z-coordinates within the levyne cage, are coordinated mainly by water molecules (as they are far from the bridging oxygen atoms), and C5 (Merlino et al. 1975; Gatta et al. 2005), in the center of the single 6mR ⊥ (0001) window shared by two levyne cages, coordinated only to framework oxygen atoms.

EXPERIMENTAL SECTION

The levyne sample (s.g. $R\bar{3}$m) used in this work originated from Fagridalur (Iceland). The chemical formula is $(Ca_{7.8}\ Na_{2.2}K_{1.1})_{\Sigma 11.1}Al_{20}Si_{34.2}O_{108}{\cdot}51.5H_2O$ (Galli et al. 1981) and the cell parameters are $a = 13.3770(4)$ Å, $c = 22.870(1)$ Å, $V = 3544.1(3)$ Å^3 (this work, Table 1).

Data collection

Single crystal XRD experiments (SC-XRD) were performed using a Philips PW1100 four-circle automated diffractometer equipped with a point detector working with graphite monochromatized Mo*K*α radiation at 30 mA/50 kV and using a 0.5 mm collimator, and operated with FEBO software (a locally developed control software). The diffractometer is equipped with a microfurnace for in-situ high-temperature experiments consisting of an H-shaped Pt-Rh heating element and a Pt:Pt-Rh thermocouple inside a cylindrical steel cage, 1 inch wide, closed with a Kapton film. The device allows the collection of diffraction data up to θ max=29°.

A crystal with sharp extinction was loaded in a 0.3 mm inner diameter pure-SiO_2 vial, 26 mm long, welded at the top using an oxy-methane flame. The crystal was kept in position within the vial using SiO_2 wool, to avoid any mechanical stress. A temperature calibration of the microfurnace was undertaken by observing the melting of eight selected pure salts and measuring the thermal expansion of a spherical quartz crystal across the α-β phase transition, mounted as described in Cámara et al. (2012). Lattice constants (Table 2a and Figure 2) were determined using the Philips LAT procedure based on the least-squares refinement of the UB-matrix on the basis of selected intense reflections in the θ-range 2-27°, at intervals of 25 °C in the *T* range 30-250 °C. The crystal was then kept in isothermal condition at 225 and 250 °C and the lattice parameters were refined at different heating times as they continuously changed. These isothermal data are reported in Figure 2 (the evolution of volume cell in isothermal collections are labeled with 1-5). Intensity data collections were performed at 30, 100, and 250 °C. Profiles of 2.1° in ω at a fixed scan rate of 0.07°sec^{-1} were integrated using the Lehman and Larsen (1974) method, and intensities were corrected for Lorentz and polarization effects and absorption using a ϕ-scan method (North et al. 1968). After reaching 250 °C the crystal was cooled, dismounted from the quartz vial and a complete data collection was carried out at room temperature (r*T*- rev) using a Bruker-AXS 3-circle diffractometer equipped with a SMART APEX CCD detector (graphite-monocrhromatized MoKα radiation λ=0.71073 Å, 50 kV, 30 mA) and a MonoCap collimator. The Bruker SMART v.5.625 software package was used for the collections of images. A total of 3360 frames (frame resolution 512x512 pixels) were collected with four different goniometer settings using the ω-scan mode (scan width: 0.2°ω; exposure time: 15 s; detector sample distance 5.02 cm). Completeness of the measured data was achieved up to 50° 2θ. The Bruker SAINT+ v.6.45 software was used for data reduction, including intensity integration and background and Lorentz-Polarization corrections. Semi-empirical absorption correction was applied using the SADABS program (Sheldrick 1996).

The temperature-resolved X-ray powder diffraction experiment (SR-XRPD) was performed at the GILDA beam line (European Synchrotron Radiation Facilities, Grenoble, France). The powdered sample of levyne was carefully packed inside a 0.5 mm quartz capillary open at both ends. Data were acquired in parallel Debye-Scherrer geometry, with a wavelength of 0.95337 Å; the rotating capillary sample was heated in-situ by means of hot air stream equipment, with a heating rate of 5°C/min. The wavelength was calibrated using LaB6 as external standard, while temperature calibration was achieved by measuring the thermal expansion of alumina standard collected in the same experimental conditions. The patterns were collected every 25°C from room-*T* (r*T*) to 958°C, on an image plate detector MAR345. A total of 42 diffraction images were collected and integrated using Fit2D software (Hammersley, 1996). To test the rehydration effect, 7mg of levyne powder was heated using a Seiko SSC/5200 thermogravimetrical instrument, operating at 5 °C/min heating rate, from r*T* to 600 °C. After 1 week, a further TG analysis was performed and a powder pattern was collected on a Panalytical X-'Pert Pro laboratory diffractometer at the Centro Interdipartimentale Grandi Strumenti of the University of Modena and Reggio Emilia (Cu*K*α radiation, θ-θ Bragg Brentano geometry, 0.02 step scan on the angular range 3-100° 2θ).

Structural refinement

SC-XRD

X-ray structure refinements against F^2 were performed in the s.g. $R\bar{3}m$ using the SHELX-97 (Sheldrick 2008) program, starting at r*T* from the atomic coordinates of Gatta et al. (2005). Scattering factors were from the International Tables for X-ray Crystallography (Wilson, 1995). T1 and T2 sites were refined with a mixed Si65/Al35 occupancy, while extraframework cation sites were refined with a Ca scattering curve. Anisotropic displacement parameters were refined for all the framework atomic sites except for T1 and O4, while extraframework cations and water oxygen atoms sites were refined isotropically (except for C1, C5, and W1). The Platon/TwinRotMat software (Spek 2003) indicated the possible presence of a twinned crystal resulting from a two-fold rotation around $[\bar{1}10]$, which, added to the model, resulted in a 90:10(1) ratio. The volume of the largest suitable crystal (0.300 x 0.200 x 0.125 mm) was not enough to get good statistics (ca. 1/3 total number of reflections had $I > 4\ \sigma(I)$) considering the high backgrounds due to the mounting of the crystal (scattering of amorphous SiO_2). At 250°C the data obtained from integrating profiles were far too weak to try to solve the structure. Profiles were extremely broad (up to 4°) and with high background due to the SiO_2 vial and wool. Only 60 reflections had $I > 4\ \sigma(I)$, hence it was decided to cool the crystal, extract it from the vial and try a data collection at r*T* with a more sensitive detector. In the new data collection the images showed the presence of frequent streaking along [00.1] caused by the presence of diffraction domains with different *c* parameters. Reflections that were weak or absent in the experiments performed at temperatures < 250 °C, now resulted intense; however, all the diffraction peaks were broad. This situation, already observed in the data collected during heating at 250°C, is probably due to the mosaicity caused by the dehydration and preserved after cooling. The refined lattice parameters were in agreement with those found at 250°C - the cell is compressed in the (00.1) plane and expanded along [00.1], compared to the original levyne - indicating that cooling does not influence cell size (see Table 2a and Fig. 2). The structural refinement, carried out using the levyne structure, yielded high agreement factors and three new strong maxima, close to the T1 site, were found in the Fourier difference map. The presence of these new sites was compatible with the breaking of T-O-T bridges and the formation of new tetrahedra, with two oxygen atoms common to the previously occupied sites, in an “edge-sharing” relationship with the original tetrahedra. These new sites (called T1B, OB1, and OB2) were added to the LEV model. Both these new sites and the original T1, O2, and O3 sites were refined with variable occupancy factors. In this way a reasonable *R*-index was obtained (Table 1). As discussed in details below, this final geometry is compatible with the presence of two mutually exclusive tetrahedra sharing an edge.

Three new extraframework cation sites (C5B, C6, and C7) were located in the Fourier difference map, along with three water sites (W5, W6, W7) coordinating framework oxygen atoms, related to rehydration at room conditions. The new T1B tetrahedra together with the T2 tetrahedra form a new framework type (see details in the next section), coexisting with the LEV structure in an epitactic relation, since both have parallel lattice parameters. It is assumed that part of the volume of levyne has reacted forming the new framework in a discontinuous, but pervasive, fashion.

Details of the data collection and structure refinements at room temperature (r*T*), 100 °C and again at room temperature (r*T*-rev) after cooling are reported in Table 1. Atom coordinates, refined site occupancies and isotropic displacement parameters are reported in Table 3a. Selected interatomic distances and angles are reported in Table 4. Anisotropic displacement parameters are available from electronically archived CIF files. Lists of observed and calculated structure factors are available from the authors.

SR-XRPD

The GSAS package (Larson and Von Dreele 2000) with the EXPGUI (Toby 2001) interface was used for Rietveld profile fitting. The cell parameter were refined on 31 patterns, covering the T range r*T*- 708 °C. A complete structural refinement was performed by means of the Rietveld method on 15 selected patterns (14 up to 266 °C and at 458 °C). The bad peak to background ratio and the broadening of the diffraction peaks did not allow satisfactory refinements at higher temperature.

The extracted Bragg peak profiles were modeled by a pseudo-Voight function with 2 refined coefficients (one Gaussian and one Lorentian term, Gw and Ly in GSAS terminology) and a 0.01 % peak intensity cut-off. The background curve was fitted with a 20 refined coefficient Chebyshev polynomial. Soft-constraints were applied to the T-O distances and gradually released after the initial stages of refinement. The thermal displacement parameters were constrained in the following way: the same value for all tetrahedral atoms, a second one for all framework oxygen atoms, a third one for extraframework cations, and a last one for water molecules.

In the final cycles, the refined structural parameters for each data histogram were the following: fractional coordinates for all atoms; occupancy factors for extraframework cations, water oxygen and partially occupied framework atoms; thermal isotropic displacement factors. Occupancy factors and isotropic thermal displacement parameters were varied in alternate cycles. Scattering factors for neutral atoms are those listed by Cromer and Waber (1974).

At r*T*, the structure determined by Gatta et al. (2005) at ambient conditions was used as a starting model for the framework atoms, whereas the extraframework sites were located using the differences Fourier map. Based on this structural model, the Rietveld refinements converged successfully up to 266 °C. At 308 °C the appearance of some new diffraction peaks indicated the occurrence of a new unknown phase (hereinafter called *levyne B*). The two phases levyne and *levyne B* coexist up to 408 °C. Above 433 °C, levyne completely disappears. The *levyne B* structure has the same s.g. of levyne and was successfully refined from the pattern collected at 458 °C, starting from the framework coordinates obtained in the single crystal experiment at r*T* after cooling (r*T*-rev). The extraframework sites C5B and C7 were absent in this refinement, but two different cationic sites (C8 and C9) were located in the Fourier difference map. No residual water molecules were found in the channels at this temperature. This structural model was used along with that of levyne refined at 266

°C in a two-phase Rietveld refinement, aimed at determination of cell parameters in the T range 308-408 °C.

Table 2b and Figure 2 report the unit cell parameters up to 708 °C. The details of the structural refinements performed at r*T*, 266 and 458 °C are reported in Table 1. Figure 3 shows the corresponding diffraction patterns. The refined atomic coordinates, occupancy factors and thermal parameters for the structures at the selected temperatures are reported in Table 3b; the bond distances are provided in Table 4.

RESULTS

While the unit cell parameters were successfully determined from r*T* to 708 °C in the SR-XRPD experiment, the structure refinements were only carried out in the range r*T* - 266 °C and at 458 °C because, during the phase transition (i.e. between 266 and 408 °C), the presence of both levyne and *levyne B* phases prevented a correct structural analysis. Figure 2 and Table 2b (reporting the variation of the cell parameters as a function of temperature) show that, below 100°C, a lattice parameter slightly increases, c decreases, and the cell volume undergoes a very small reduction (<1%). In the range 100–283°C a decreases and c increases, accounting for a V reduction of ~ 2%. At 308 °C, the phase transition to the new phase *levyne B* is accompanied by rather sharp decreases of a and V, while the c parameter remains almost constant. The two phases coexist up to 408 °C. Above this temperature only *levyne B* is present and small variations in the cell parameters occur up to the highest investigated temperature. Overall, the variations of the unit cell parameters are: $\Delta a = -5\%$, $\Delta c = +3\%$, $\Delta V = -7\%$.

Data obtained from the single crystal experiment show that the lattice variations take place at lower temperatures (almost 100 °C lower). This phenomenon is common in zeolite dehydration studies when comparing single crystal and powder data (Cruciani 2006) and can be ascribed to the different heating conditions. The cell parameters determined in the isothermal data collections at 225 and 250 °C (Figure 2 and Table 2a) show a strong volume contraction (points 1-2) corresponding to the phase transition and to the complete dehydration of levyne. The following points (3-4-5) indicate a volume increase of 2.5% that can be interpreted as a consequence of thermal expansion undergone by the zeolite during a very long heating time (Table 2a).

Framework

In both experiments at r*T* the atomic coordinates of the levyne framework (Table 3a,b) are close to those found by Merlino et al. (1975), Sacerdoti (1996), and Gatta et al. (2005). The reported Al enrichment in the T1 tetrahedron (Sacerdoti 1996; Gatta et al. 2005) is confirmed by our refinements (T1(Al) = 32 % and T2(Al) = 15% for powder data, and T1(Al) = 36 % and T2(Al)= 27% for single crystal data following Jones (1968) (Table 4). The calculated Al content is underestimated (14.22 and 17.82 Al a.p.f.u, for XRPD and SC experiments, respectively against 19.8 from the chemical analysis) as already found by Sacerdoti (1996) and Gatta et al. (2005), and in agreement with what is reported by Alberti and Gottardi (1988). In particular the discrepancy for the SR-XRPD experiment was higher due to the soft constraints imposed to the T-O distances.

The structural refinements of the powder patterns between r*T* and 266 °C made it possible to follow the framework distortions as described below:

- D6R: it becomes more ditrigonal between r*T* and 87 °C, whereas above this *T* its ditrigonalization (expressed as the O3–O2–O3 and O2-O3-O2 angles) decreases (Figure 4 and Table 5). The variation of O1–O4–O1 angle influences the O1–O1 distance (Figure 5), which represents the D6R thickness, and this in turn is strictly related to the abovementioned *c* parameter variation (Figure 2).

- 8mR: this aperture tends to become more elliptic; in particular, the O5-O5 distance increases in all this T range, inducing the *c* axis increase, while the *a* axis trend follows that of the O4-O4 distance (Figures 6 and 2).

- 6mR: no deformations are observed in this T range.

At 308 °C the phase transition starts, with the statistically significant presence of a new framework topology. The structural features of the new phase *levyneB,* determined at 458 °C (i.e. when the phase transition is complete) are reported in Tables 3b and 4 and in Figures 7a,b. The occurrence of the new topology is associated to the following framework changes:

- T1 site occupancy factor decreases and a new tetrahedral site (T1B) and two oxygen sites (OB1 and OB2) appear (Table 3a,b); this can been interpreted as the statistical breaking of the oxygen bridges T1–O2–T1 and T1–O3–T1 in the D6R, with a frequency of about 40%;
- the tetrahedral cation migrates from T1 to the new tetrahedral site T1B (Figure 7a,b and Tables 3b and 4). The new T1B shares the oxygen atoms O1 and O4 with the previously occupied site, whereas the new vertices OB1 and OB2 are located on a mirror plane parallel to *c* and are shared by the new T1B tetrahedron of adjacent D6R units. In this way, virtually “edge-sharing” tetrahedra T1 and T1B (mutually exclusive) are formed .From the data reported in Table 4, the distortion of the new tetrahedron T1B and the *T*-induced contraction of T1 dimensions is evident.

The overall result of the dehydration process is the formation of a new framework topology – constituted by a sequence of a new zeolitic cage and two cancrinite cages superimposed along [0001] – and by the disappearance of the D6R and the 8mR units present in LEV topology (Figure 7b). The new cage can be described as a 20-hedron formed by fourteen 6mR and six 4mR. The new topology, described by the 6mR sequence **ABCBCACAB, corresponds to one of the simpler net of the ABC family enumerated by Smith and Bennett (1981). In Table 1 of that paper the authors report that only 2 9-layers (3-layers rombohedral) sequences exist: AABCCABBC (corresponding to levyne) and ABCBCACAB (corresponding to the new topology in *levyne B*). This latter topology is also reported in the database of the hypothetical ABC-6 structures with the code 166_2_293 (Foster and Treacy, 2010). It must be stressed that the breaking of the LEV framework occurs only on a statistical basis. L*evyne B* is formed by both the original framework and the new topology, coexisting in percentages of about 40 and 60%, respectively**.

Starting from 308 °C and up to the highest investigated temperature, *levyne B* remains stable, and the percentage of the new topology does not change.

The main deformations undergone upon heating by the portion of the original LEV topology present in *levyne B* (Table 5) mainly regard the 8mR, with the O4–O4 and O5–O5 distances decreasing and increasing, respectively. The O1–O4–O1 angle of the D6R increases and, as a consequence, its thickness (O1–O1 distance) increases too. Finally, the 6mR become more ditrigonal. These structural variations can justify the *a* parameter decrease and *c* increase during the phase transition previously discussed (Table 2 and Figure 2).

Extraframework sites

In both experiments the distribution of cations and water molecules at r*T*, is consistent with the data reported by Gatta et al. (2005), while some differences are observed compared to the results of Sacerdoti (1996) and Merlino et al. (1975). In particular, the Na3 site of the Sacerdoti refinement (corresponding to the C(4) site in the Merlino et al. refinement) and the water sites W6 and W7 are absent in our levyne. On the basis of the electronic density and bond distances, we assume that the C1 and C2 sites are occupied by Ca, C3 by K, and C5 by Ca and Na. A total of 58.5 water molecules are localized in the SR-XRPD experiment, while only 31 in SC-XRD.

The number of electrons calculated from the powder refinement for the extraframework cation sites (178 e^-) and water sites (468 e^-) is lower and higher, respectively, than as derived from chemical analysis (201 $e^-$for the extraframework cations and 414 for the water molecules) (Galli et al. 1981). On the contrary, while the number of water molecules located in the SC-XRD experiment is very low (31 molecules accounting for 247 e^-), the number of electrons pertaining to cationic sites (205) is consistent with the chemical data. In the thermo gravimetric analysis reported here (Figure 8) the total water loss is 19.8 wt.%, corresponding to 50 water molecules (i.e. 400 e^-).

The dehydration process can be followed on the basis of XRPD structure refinements. Between r*T* and 266 °C, 23 water molecules are lost (Figure 9a and b), three of which already below 100 °C. The other 35.5 molecules are lost during the phase transition (in the *T* range 266-458 °C), so that *levyne B* is completely anhydrous (Tables 3a,b, Table 4, and Figures 7a,b). In detail: *i)* W3 is the first molecule to leave the zeolite porosity and is completely lost before the phase transition; *ii)* W2 is the second water site which decreases its occupancy already below 100 °C, while W1 and W4 are partially released above 180 °C; *iii)* at 266 °C the occupancy factors of the W1, W2, and W4 sites are still 0.70, 0.61, and 0.35, respectively. The thermo gravimetric curve reported in Figure 8 shows that up to 250 °C 35 water molecules (14 wt.%) are released; this number is higher than that found from the refinement. However, this apparent discrepancy can be reasonably explained by the different experimental set up adopted in the two measurements (powdered sample in a small open platinum boat in the TG apparatus, and in a glass capillary in the SR- XRPD experiment).

The evolution of the extraframework cation sites between r*T* and 266 °C (Figure 10, and Tables 3b and 4) is as follows: *i)* C2 site, initially coordinated only to water molecules (W1, W2, W3), disappears already below 100 °C; *ii)* as a consequence, the calcium atoms move towards the C1 and C5 sites - which are strongly bonded to the framework oxygen atoms - to achieve improved coordination; *iii)* as a result, the occupancy factor of C5 increases and C1 becomes completely occupied; *iv)* the occupancy factor of the C3 site slightly decreases.

At 458 °C the structural refinement of *levyne B* shows that the C1 site splits over three positions (C1, C6, and C9). C1 corresponds roughly to the original site, C6 is located at the center of the D6R, and C9 is near the center of the 6mR forming the D6R (Tables 3b and 4). Moreover, a new site (C8) is found along the cage walls. The cation site C3 shifts towards a position near to the C2 site of the r*T* structure, while the occupancy of C5 decreases down to the r*T* value.

Hence, in the *levyne B* structure, the cations are distributed in the following way (Figure 7a,b):

- C1 is present only in the portion with LEV topology;
- C3 is present only in the portion with the new topology;

- C5, present in both LEV and new topology portions, is at the center of the 6mR, but in the new topology this 6mR is shared by two cancrinite cages;
- C6 (in the center of D6R) and C9 (inside the D6R) are present only in the LEV topology portion because the D6R no longer exists in the new topology;
- C8 is present in both portions.

Reversibility

The powder pattern collected on the levyne sample one week after dehydration by TG treatment revealed that the phase transition to *levyne B* is only partially reversible. In fact, very weak *levyne B* peaks are recognizable in the pattern, while levyne is the dominant phase. The refinement of the unit cell indicates that the parameters of *levyne B* roughly correspond to its parameters collected during heating between 333 and 358°C (corresponding with the first appearance of *levyne B*). Regarding levyne, even if the cell volume corresponds roughly to the volume at r*T*, the parameters *a* and *c* remain contracted and expanded, respectively, showing values compatible with those refined at 194 and 230°C, respectively. The partial regain of unit cell parameters indicates a partial rehydration of the sample. This is confirmed by the results of the TG analysis (Figure 8) performed on the rehydrated sample, showing a water loss of 14% against the 19.8 % of the original sample (regain of 29.5 molecules on 50 of the original sample). This effect is also consistent with the findings of the SC experiment collected after cooling (rev). The refinement shows a contracted cell (even if larger than that found for *levyne B* at 458 °C) and the presence of 18.2 water molecules in the channels, indicating partial rehydration. This value is lower than that found in TG experiment since the SC-XRD pattern was collected only one day after the high temperature treatment.

DISCUSSION

The main driving force for *levyne B* formation is the strain induced on the T1–O2–T1 and T1–O3–T1 bridges by the calcium atoms which, migrating from the C1 site towards the C6 site at the center of the D6R in response to dehydration, strongly interact with these oxygen atoms (Table 4). Furthermore, it is worth noting that OB1, one of the new oxygen atoms coordinating the new T1B "*edge sharing*" tetrahedron, is near to the W2 site of the original levyne structure.

The influence of water in the bridge breaking and mobility of the tetrahedral atoms has been discussed in depth (Meier and Groner 1981, Alberti and Vezzalini 1984). Literature reports that water – in particular protons – represents a necessary catalyst for these topological changes. At *HT*, the framework oxygen atoms originally coordinating extraframework cations are attacked by the protons of the water molecules. As a consequence, the corresponding T-O-T bridge is broken allowing the tetrahedral cations to migrate to a new position. The new tetrahedron has three vertices in common with the previously occupied tetrahedron, and a fourth vertex as an oxygen atom when shared by two tetrahedra, or an hydroxyl when unshared.

The high temperature behaviour of levyne is consistent with that observed for other zeolites characterized by the temperature-induced T–O–T bridge breaking. In fact, in all cases up to now reported in literature, the breaking invariably occurs in the smallest ring present in the framework. (Alberti and Martucci 2011).

It is interesting to note that in the *levyne B* structure, after complete dehydration, no further bridge breaking occurs, i.e. the occupancy of the sites T1B, OB1, and OB2 does not change with increasing temperature. This could be due to the complete lack of water molecules in the channels; if some molecules remained as catalysts, probably 100% of the structure would undergo bridge breaking and transform into the new framework.

The variation of the lattice parameters observed in the temperature range between 300 °C and 400 °C, corresponding to the formation of *levyne B,* can be justified taking into account the metrical aspects of double and single six-membered rings of tetrahedra (Gard and Tait 1972; Merlino 1984). It is known in fact that double and single rings have different lateral dimensions. In 6mR one edge of each tetrahedron is vertical, whereas in D6R the base of each tetrahedron is

nearly normal to the c axis. The sudden decrease of a parameter can be interpreted as a consequence of the formation of the new topology in *levyne B* where only single 6mR are present.

Classification of levyne thermal behavior

Levyne could be classified in the category 3 identified by Alberti and Vezzalini (1984), exhibiting complete dehydration accompanied by topological changes in the framework, as a consequence of T–O–T breaking. In general, as discussed in the review paper of Cruciani (2006), several factors may control zeolite thermal behavior:

i) Si/Al ratio of the framework (thermal stability increases with the Si/Al ratio);
ii) the number, ionic potential and size of the exchangeable cations (zeolites containing monovalent cations are more stable than those containing divalent ones);
iii) the coordination of bare cations after water expulsion;
iv) the framework topology.

The thermal behavior of the levyne sample studied here perfectly fits literature data, with its low Si/Al ratio (1.6) and the predominant presence of calcium as extraframework cation. Several authors have reported that the drop in Ca coordination below a critical point after water expulsion can be regarded as a cause of zeolite structural breakdown. This aspect is evident in several Ca-bearing zeolites that appear unstable when the Ca coordination number is lower than six or seven (Ståhl and Hanson 1994; Vezzalini et al. 1999). Unfortunately, the impossibility of obtaining reliable structural refinements of levyne between 283 and 433 °C made it impossible to follow the complete release of water molecules and, as a consequence, to explore the changes of Ca coordination in detail.

Comparison with literature data

T-O-T bridge breaking has been observed in other zeolites with a framework characterized by D6R units. In the (Na, TMA)-form of the synthetic zeolite EAB (Meier and Groner, 1981), at about 360 °C the breaking of three bridges of one of the 6mR of the D6R – associated with the migration of the tetrahedral cations of two adjacent D6R and the formation of new T-O-T bridges – leads to the formation of a *sodalite*-type phase with a new 6mR sequence (from the original ABBACC to the new ABCABC). Similarly, when Li-Losod – characterized by a 6mR sequence ABAC – is treated with a dilute LiOH solution, it transforms into Li-cancrinite – characterized by a ABAB sequence (Sieber and Meier 1974). This is due, once again, to the breaking of T–O–T bridges in one 6mR. It is also interesting to note that, in both these phases, T–O–T breaking involves the bridges on the plane of the 6mR, as occurs in levyne.

It is also interesting to compare our data on natural levyne with the thermal behavior of a synthetic boron levyne, containing quinuclidine as a template, studied in the 25–900 °C T range (Leardini et al. 2013). Above 500 °C a dramatic change in the unit-cell parameters was identified and attributed to the decomposition and expulsion of organic molecules. Moreover, the evolution of the T-O bond distances and O–T1–O angles indicated the formation of boron in triangular planar coordination, in very close agreement with the NMR and FTIR analyses reported by Millini et al. (1992). In particular the authors compared the mean value of the O–T1–O angles at the base of tetrahedron T1 [<O–T1–O>base=(O1–T1–O2 + O1–T1–O3 + O2–T1–O3)/3] with those involving the apical oxygen [<O–T1–O>apical = (O1–T1–O5 + O2–T1–O5 + O3–T1–O5)/3]. They found an enlargement of the <O–T1–O> base angle (from 109.3° at 550 °C to about 114° at 800 °C) and the corresponding shrinkage of the <O–T1–O> apical angle involving the O5 apical oxygen (from 109.6° at 550 °C to about 105° at 800 °C). These results have been interpreted as a trend in the structure towards the formation of a triangular planar coordination of boron. On the basis of the present study, this behavior could be interpreted as the breaking of a T-O-T bridge and the formation of an interrupted framework with a BO_3 and a $TO_3(OH)$ tetrahedron. This effect could be induced by template loss and the formation of a hydrogenated form of levyne. The hydrogen would attract the O5 oxygen, leaving the boron in a triangular coordination.

CONCLUDING REMARKS

The high temperature study carried out on the zeolite levyne evidenced that above 300 °C a phase transition (to the so-called *levyne B*) occurs. This phenomenon is the consequence of the breaking of oxygen bridges and gives rise to a new topology. *Levyne B* derives from the coexistence of the original levyne topology (present in 60% of cases) and a new topology (present in 40% of cases). The 8mR bidimensional channel system of levyne is absent in the new topology. A crucial consequence of the formation of the phase B for levyne technological applications is the closure of the bidimensional channel system in the new topology, with consequent hindering of molecular diffusion at high temperature.

ACNOWLEDGEMENTS

BM08 (GILDA-CRG) beamline at European Synchrotron Radiation Facility is acknowledged for allocation of the experimental beamtime. The authors are indebted with Francesco D'Acapito and Angela Trapananti for their assistance during the diffraction experiments. Dr. Simona Bigi is acknowledged for the TG analyses. This work was supported by the Italian MIUR (PRIN 2008, PRIN 2009). FC thanks ex 60% 2012 D15E12002540005 "*Thermal expansion of cancrinite group minerals*". Stefano Merlino and an anonymous reviewer are acknowledged for the useful comments, which greatly contributed to improve the quality of the paper.

References

Alberti, A. (1972) On the crystal structure of the zeolite heulandite. Tschermaks Mineralogische Petrographische Mitteilungen, 18, 129–146.

Alberti, A. (1973) The structure type of heulandite B (heat-collapsed phase). Tschermaks Mineralogische Petrographische Mitteilungen, 19, 173–184.

Alberti, A. and Gottardi, G. (1988) The determination of Al-content in the tetrahedra of framework silicates. Zeitschrift für Kristallographie, 184, 49–61.

Alberti, A. and Vezzalini, G. (1978) Crystal structures of heat-collapsed phases of barrerite. In L.B. Sand and J.Mumpton Eds., Natural zeolites. Occurrence, properties, use, pp. 85-98, Pergamon Press, Oxford and New York.

Alberti, A. and Vezzalini, G. (1983) The thermal behaviour of heulandites: structural study of the dehydration of Nadap heulandite. Tschermaks Mineralogische Petrographische Mitteilungen, 31, 259-270.

Alberti, A. and Vezzalini, G. (1984) Topological changes in dehydrated zeolites: breaking of T-O-T oxygen bridges. In D. Olson and A.Bisio, Eds., Proceedings of the 6th International Zeolite Conference, Reno, 834-841, Butterworths, Guildford, U.K.

Alberti, A. and Martucci, A. (2011) Reconstructive phase transitions in microporous materials: Rules and factors affecting them. Microporous and Mesoporous Materials, 141, 192-198.

Alberti, A. and Martucci, A. (2005) Phase transformations and structural modifications induced by heating in microporous materials. Studies in Surface Science and Catalysis, 155, 19-43;

Alberti, A., Cariati, F., Erre, L., Piu, P., and Vezzalini, G. (1983) Spectroscopic investigation on the presence of OH in natural barrerite and in its collapsed phases. Physics and Chemistry of Minerals, 9, 189-191.

Alberti, A., Rinaldi, R., and Vezzalini, G. (1978) Dynamics of dehydration in stilbite-type structures: Stellerite Phase B. Physics and Chemistry of Minerals, 2, 365-375.

Alberti, A., Sacerdoti, M., Quartieri, S., and Vezzalini, G. (1999) Heating-induced phase transformation in zeolite brewsterite: new 4- and 5-coordinated (Si,Al) sites. Physics and Chemistry of Minerals, 26, 181-186.

Alberti, A., Vezzalini, G., Cariati, F., Erre, L. and Piu, P. (1985) Dehydration and re-hydration of the zeolites with 4-4-1 SBUs: near IR evidence for topological changes in heulandite. Zeolites, 5, 289-291.

Alberti, A., Vezzalini, G., Quartieri, S., Cruciani, G., and Bordiga, S. (2001) Rehydration mechanisms in zeolites: reversibility of the TOT breaking and tetrahedral cation migration in brewsterite. Microporous and Mesoporous Materials, 42, 277-287.

Alberti, A., Parodi, I., Cruciani, G., Dalconi, M.C., Martucci, A. (2010) Dehydration and rehydration processes in gmelinite: an in situ X-ray single-crystal study. American Mineralogist, 95 1773-1782.

Arletti, R., Mazzucato, E., and Vezzalini, G. (2006) Influence of dehydration kinetics on the T-O-T bridge breaking in zeolites with framework type STI: the case of stellerite. American Mineralogist, 91, 628-634.

Armbruster, T. (1993) Dehydration mechanism of clinoptilolite and heulandite: single-crystal X-ray study of Na-poor, Ca-, K-, Mg- rich clinoptilolite at 100 K. American Mineralogist, 78, 260-264.

Armbruster, T. and Gunter, M.E. (1991) Stepwise dehydration of heulandite-clinoptilolite from Succor Creek, Oregon, U.S.A.: a single-crystal X-ray study at 100K. American Mineralogist, 76, 1872-1883.

Barrer, R.M. and Kerr, I.S. (1959) Intracrystalline channels in levynite and some related zeolites. Transaction of the Faraday Society, 55, 1915-1923.

Bish D.L. and Carey J. W. (2001) Thermal behavior of natural zeolites. In: D.L. Bish and D.W. Ming (Eds.), Natural Zeolites: Occurrence, Properties, Applications, Reviews in Mineralogy and Geochemistry, MSA, vol. 45, pp. 403–452.

Brewster, D. (1825) Description of levyne, a new mineral species. Edinburgh Journal of Science, 2, 332-334.

Cámara, F., Gatta, D., Meven, M., Pasqual, D. (2012) Thermal expansion and high temperature structure evolution of zoisite by single crystal X-ray and neutron diffraction. Physics and Chemistry of Minerals, 39, 27–45.

Cartlidge, S. and Meier, W.M. (1984) Solid state transformations of synthetic CHA-and EAB- type zeolites in the sodium form. Zeolites, 4, 218-225.

Cromer, D.T. and Waber, J.R. (1974) Atomic scattering factors for X-rays. In: International Tables for X-Ray Crystallography, Vol. IV, Section 2.2, pp. 99-101. The Kynoch Press: Birmingham, U.K.

Cruciani, G. and Zanella, A. (2002) Dehydration dynamics of wairakite by in situ synchrotron powder diffraction. 18th IMA General Meeting, Edinburgo (UK), 1-6 Settembre 2002.

Cruciani, G. (2006) Zeolites upon heating: factors governing their thermal stability and structural changes. Journal of Physics and Chemistry of Solids, 67, 1973–1994.

Cruciani, G., Artioli, G., Gualtieri, A., Stahl, K., and Hanson, J.C. (1997) Dehydration dynamics of stilbite using synchrotron X-ray powder diffraction. American Mineralogist, 82, 729-739.

Flanigen, E.M., Lok, B.M., Patton, R.L. and Wilson, S.T. (1986) Aluminophosphate molecular sieves and the periodic table. Pure and Applied Chemistry, 58, 1351-1358.

Foster M.D. and. Treacy M.M.J (2010) A Database of Hypothetical Zeolite Structures: http://www.hypotheticalzeolites.net

Gard J.A. and Tait J.M. (1972) The crystal structure of the zeolites offretite $K_{1.1}Ca_{1.1}Mg_{0.7}[si_{1.8} Al_{5.2} O_{36}]15.2H_2O$. Acta Crystallographica, B28, 825-834.

Galli E. and Gottardi, G. (1966) The crystal structure of stilbite. Mineralogica and Petrographica Acta, 12, 1-10.

Galli, E. and Alberti, A. (1975) The crystal structure of stellerite. Bulletin de la Société Francoise de Minéralogie et de Cristallographie, 98, 11-18.

Galli, E. and Alberti, A. (1976) The crystal structure of barrerite. Bulletin de la Société Francoise de Minéralogie et de Cristallographie, 99, 331-340.

Galli E., Rinaldi, R. and Modena, C. (1981) Crystal chemistry of levynes. Zeolites, 1, 157-160.

Gatta, G.D., Comodi, P., Zanazzi, P.F., and Boffa Ballaran T. (2005) Anomalous elastic behavior and high-pressure structural evolution of zeolite levyne. American . Mineralogist, 90, 645-652.

Gottardi, G. and Galli, E. (1985) Natural Zeolites, vol. 18, Springer-Verlag.

Hammersley, A.P., Svensson, S.O., Hanfland, M., Fitch, A.N., and Häusermann, D. (1996) Two-dimensional detector software: from real detector to idealized image or two-theta scan. High Pressure Research, 14, 235–248.

Jones, J.B. (1968) Al-O and Si-O tethraedral distance in aluminosilicate framework structures. Acta Crystallographica, B24, 355-358.

Larson, A.C. and Von Dreele, R.B. (2000) General Structure Analysis System (GSAS). ReportLAUR 86-748, Los Alamos National Laboratory, Los Alamos, New Mexico.

Lehmann, M. S., Larsen, F. K. (1974). A method for location of the peaks in step-scan measured Bragg reflexions. Acta Crystallographica, A30, 580-584.

Leardini L., Martucci, A., Alberti, A., Cruciani, G. (2013) Template burning effects on stability and boron coordination in boron levyne studied by in situ time resolved synchrotron powder diffraction. Microporous and Mesoporous Materials, 167, 117-126.

Lok, B.M., Messina, C.A., Patton, R.L., Gajek, R.T., Cannan, T.R., Flanigen, E.M., US Patent 4440,871 assigned to Union Carbide (1984).

Meier, W.M. and Groner, M. (1981) Zeolite structure type EAB: crystal structure and mechanism for the topotactic transformation of the Na, TMA form. Journal of Solid State Chemistry, 37, 204-218.

Merkle, A.B. and Slaughter, M. (1968) Determination and refinement of the structure of heulandite. American Mineralogist, 53, 1120–1138.

Merlino, S. (1984) Recent results in structural studies of zeolites and zeolites-like materials. In D. Olson and A.Bisio, Eds., Proceedings of the 6th International Zeolite Conference, Reno, 747-759, Butterworths, Guildford, U.K.

Merlino, S., Galli, E., and Alberti, A. (1975) The crystal structure of Levyne. Tschermaks Mineralogische und Petrographische Mitteilungen, 22, 117-129.

Millini, R., Carati, A., and Bellussi, G. (1992) Synthesis of a new porous borosilicate with the levyne structure. Zeolites, 12, 265-268.

Mortier, W.J. (1983) Thermal stability of the stilbite-type framework: crystal structure of the dehydrated sodium/ammonium exchange form. American Mineralogist, 68, 414-419.

Norby, P. (1990) Thermal transformation of zeolites Li-A(BW). The crystal structure of γ-eucriptite, a polymorph of $LiAlSiO_4$. Zeolites, 10, 193-199.

North ACT, Phillips DC, Mathews FS (1968) A semi-empirical method of absorption correction. Acta Crystallographica, A30, 580–584.

Sacerdoti, M. (1996) New refinements of the crystal structure of levyne using twinned crystals. Neues Jahrbuch für Mineralogie Monatshefte, 3, 114-124.

Sacerdoti, M., Vezzalini, G., and Quartieri, S. (2000) Dehydration mechanism in brewsterite: single crystal X-ray diffraction study. Microporous and Mesoporous Materials, 41, 107-118.

Seryotkin, Y.V., Joswig, W., Bakakin, V., Belitsky, I.A., and Fursenko, B.A. (2003) High-temperature crystal structure of wairakite. European Journal of Mineralogy, 15, 475-484.

Sheldrick, G.M. (1996) SADABS, A Program for Absorption Correction with the Siemens SMART System; University of Gottingen: Gottingen, Germany

Sheldrick, G.M. (2008) A short history of SHELX. Acta Crystallographica, A64, 112–122.

Slaughter, M. (1970) Crystal structure of stilbite. American Mineralogist, 55, 387-397.

Sieber, W. and Meier, W.M.(1974) Formation and properties of losod, a new sodium zeolite. Helvetica Chimica Acta, 57, 1533–1549.

Smith, J.W. and Bennett, J.M. (1981) Enumeration of 4-connected 3-dimensional net and classification of framework silicates: the infinite set of ABC-6 nets; the Archimedean and σ-related nets. American Mineralogist, 66, 777-788.

Spek A.L. (2003) Single-crystal structure validation with the program PLATON. Journal of Applied Crystallography, 36, 7-13.

Ståhl, K. and Hanson, J.C. (1994) Real-time X-ray synchrotron powder diffraction studies of the dehydration processes in scolecite and mesolite. Journal of Applied Crystallography, 27, 543-550.

Ståhl, K. and Hanson, J.C. (1999) Multiple cation sites in dehydrated brewsterite. An in-situ X-ray synchrotron powder diffraction study. Microporous and Mesoporous Materials, 32, 147-158.

Toby, B.H. (2001) EXPGUI, a graphical user interface for GSAS. Journal of Applied Crystallography, 34, 210-213.

Vezzalini, G., Alberti A., Sani, A., Triscari, M., (1999) The dehyration process in amicite. Microporous and Mesoporous Materials, 31, 253-262.

Wadoski, E., Armbruster, T., Lazic, B., Fisch, M. (2011) Dehydration of the natural zeolite goosecreekite $CaAl_2Si_6O_{16}\cdot 5\ H_2O$ upon stepwise heating: A single-crystal and powder X-Ray study. American Mineralogist, 96, 1070–1078.

Wilson, AJC (1995) International tables for crystallography, vol C. 876 Kluwer Academic Publishers, Dordrecht.

Yamamoto, K., Ikeda, T., Onoder, M., Muramatsu, A., Mizukami, F., Wang, Y., and Gies, H. (2010) Synthesis and structure analysis of RUB-50, an LEV-type aluminosilicate zeolite. Microporous and Mesoporous Materials, 128 ,150-157.

Zhu, G.S., Xiao, F.S., Qiu, S.L., Hun, P.C., Xu, R.R., Ma, S.J. and Terasaki, O. (1997) Synthesis and characterization of a new microporous aluminophosphate with levyne structure in the presence of HF. Microporous and Mesoporous Materials, 11, 269-27.

Table captions

Table 1. Experimental data and refinement parameters for levyne at r*T*, 100 °C, and r*T* (rev) for SC-XRD experiment, and at r*T*, 266, and 458 °C for SR-XRPD experiment (rev= room temperature, collected after cooling).

Table 2. Unit cell parameters of levyne: (a) SC-XRD data; (b) SR-XRPD data (rev= room temperature, collected after cooling).

Table 3. Fractional coordinates, thermal parameters, and occupancy factors for levyne at: (a) r*T*, 100°C, and r*T* (rev) for SC-XRD experiment; (b) rT, 266, and 458°C for SR-XRPD experiment (rev= room temperature, collected after cooling).

Table 4. Interatomic distances (shorter than 3.2 Å) for levyne at: (a) rT, 100°C, and rT (rev) for SC-XRD experiment; (b) rT, 266, and 458°C for SR-XRPD experiment (rev= room temperature, collected after cooling).

Table 5. Selected distances characterizing the levyne framework (D6R, 8mR, 6mR) as a function of temperature. In grey *levyne B* framework features. Data taken from SR-XRPD structure refinements.

Figure captions

Figure 1. Projection along [001] of levyne structure (a) and view of extraframework sites in the levyne cages (b) at r*T*.

Figure 2. Plot of normalized unit cell parameters of levyne *vs*. temperature for SC-XRD and SR-XRPD experiments. Number 1-5 indicate the cell volume sequence from SC-XRD isothermal data collections at 225 and 250°C. Points 2 and 3 are almost overlapped.

Figure 3. X-ray powder diffraction patterns collected on levyne at r*T*, 266, and 458 °C in the range 3-20 °2Θ.

Figure 4. Structural features of the D6R *vs*. temperature: internal angle O3-O2-O3 and O2-O3-O2 (data from SR-XRPD experiment).

Figure 5. Structural features of the D6R *vs*. temperature: O4-O1-O4 angle variations and O1-O1 (thickness of D6R) variations (data from SR-XRPD experiment).

Figure 6. Structural features of the 8-ring *vs*. temperature: O4-O4 and O5-O5 distances (data from SR-XRPD experiment).

Figure 7. Structure of *levyne B*: (a) LEV framework; (b) new topology.

Figure 8: Thermogravimetric analyses performed on natural levyne (solid line) and on the dehydrated/rehydrated sample (dotted line).

Figure 9. (a) Occupancy factors of W sites, and (b) total water content *vs*. temperature (data from SR-XRPD experiment).

Figure 10. Occupancy factors of extraframework cation sites *vs*. temperature (data from SR-XRPD experiment).

	SC-XRD			**SR-XRPD**		
T (°C)	**r*T***	**100°C**	**r*T* (rev)**	**r*T***	**266 °C**	**458 °C**
Space Group	$R\bar{3}m$	$R\bar{3}m$	$R\bar{3}m$	$R\bar{3}m$	$R\bar{3}m$	$R\bar{3}m$
***a* (Å)**	13.421(3)	13.3690(8)	12.8585(7)	13.3769(4)	13.2213(3)	12.7730(7)
***c* (Å)**	22.762(12)	22.760(3)	23.419(3)	22.869(1)	23.1860(9)	23.566(1)
V (Å^3)	3550.7(20)	3523.0(6)	3353.36(50)	3544.1(2)	3509.9(2)	3329.6(4)
xR_p (%)				1	1	1.1
R_{wp} (%)				2.1	1	1
R F2 (%)**				10.6	13.43	17.3
R1 (%)	10.9	8.1	12.6			
R2W (%)	23.1	21.4	31.5			
No. of variables	71	69	98	76	74	80
No. of observations	2046	2034	3662	2633	2633	2576
No. of reflections	2046	2034	761	595	590	567
R_{merge} (%)	13	12	4.7			

T (°C)	*a* (Å)	*c* (Å)	*V* (Å^3)	time (min)
25	13.421(3)	22.762(2)	3550.7(11)	0
50	13.434(2)	22.644(7)	3538.9(14)	120
75	13.410(2)	22.671(7)	3531.0(13)	240
100	13.3690(1)	22.760(2)	3523.0(3)	360
125	13.3163(1)	22.901(1)	3516.9(3)	4250
150	13.2684(1)	23.035(2)	3512.0(4)	5720
175	13.2365(1)	23.126(2)	3508.9(4)	5952
200	13.2105(1)	23.207(1)	3507.4(3)	6094
225	13.158(3)	23.327(9)	3497.6(17)	7152
225	12.789(3)	23.124(2)	3275.5(10)	8972
225	12.786(2)	23.124(3)	3274.1(8)	15812
250	12.80(11)	23.34(3)	3310(6)	20540
250	12.87(15)	23.44(2)	3360(6)	24995
25(rev)	12.87(25)	23.44(4)	3362(11)	29811

Temp (°C)	***a* (Å)**	***c* (Å)**	***V* (Å^3)**	***phase***
28	13.377(4)	22.870(1)	3544.1(3)	levyne
52	13.3924(4)	22.8091(9)	3542.8(3)	levyne
69	13.4063(3)	22.742(8)	3539.8(2)	levyne
87	13.4036(3)	22.716(7)	3534.3(2)	levyne
105	13.4022(3)	22.7245(7)	3534.9(2)	levyne
123	13.3961(3)	22.7554(8)	3536.5(2)	levyne
141	13.3700(3)	22.776(8)	3525.9(2)	levyne
158	13.3522(3)	22.8273(7)	3524.4(2)	levyne
176	13.332(3)	22.8861(8)	3522.8(2)	levyne
194	13.3096(3)	22.944(1)	3519.9(2)	levyne
213	13.2861(3)	23.0066(9)	3517.0(2)	levyne
230	13.2624(3)	23.0699(9)	3514.2(2)	levyne
248	13.2424(3)	23.1312(9)	3512.9(2)	levyne
266	13.2213(3)	23.186(9)	3509.9(2)	levyne
283	13.199(3)	23.245(1)	3507.0(2)	levyne
308	13.1694(4)	23.314(1)	3501.8(3)	levyne
333	13.1422(8)	23.404(8)	3500.8(5)	levyne
	12.932(4)	23.58(1)	3414(2)	*levyne B*
358	13.069(1)	23.443(4)	3467.7(9)	levyne
	12.830(2)	23.518(2)	3352(1)	*levyne B*
383	13.021(2)	23.441(7)	3442(1)	levyne
	12.800(1)	23.523(4)	3337.5(8)	*levyne B*
408	12.989(3)	23.45(1)	3426(2)	levyne
	12.788(1)	23.534(3)	3333.2(6)	*levyne B*
433	12.7829(7)	23.560(2)	3333.9(4)	*levyne B*
458	12.773(7)	23.566(1)	3329.6(4)	*levyne B*
483	12.7654(6)	23.574(1)	3326.9(4)	*levyne B*
508	12.7582(6)	23.58(1)	3324(3)	*levyne B*
533	12.7535(6)	23.582(1)	3321.8(3)	*levyne B*
558	12.7493(6)	23.585(1)	3320.1(3)	*levyne B*
583	12.7452(6)	23.585(1)	3317.9(3)	*levyne B*
608	12.7425(7)	23.589(1)	3317.0(3)	*levyne B*
633	12.732(1)	23.573(3)	3309(1)	*levyne B*

658	12.7385(7)	23.584(1)	3314.2(3)	*levyne B*
683	12.7380(7)	23.584(1)	3314.0(2)	*levyne B*
708	12.7347(7)	23.578(1)	3311.4(4)	*levyne B*
r*T* (rev)	13.316(1)	23.066(9)	3541.8(1)	*levyne*
	12.882(4)	23.3840(1)	3361.0(3)	*levyne B*

	r*T* (SC-XRD)				
	x/a	**y/b**	**z/c**	**F**	**Uiso**
T1 (Si)	0.0002(2)	0.2304(2)	0.0703(1)	0.63	0.0120(8)
T1 (Al)	0.0002(2)	0.2304(2)	0.0703(1)	0.37	0.0120(8)
T2 (Si)	0.2393(2)	0	½	0.63	0.0091(9)
T2 (Al)	0.2393(2)	0	½	0.37	0.0091(9)
O1	0.0367(4)	0.3496(8)	0.1079(3)	1	0.024(2)
O2	0.0898(3)	-0.0898(3)	0.0849(4)	1	0.018(2)
O3	0.1277(4)	-0.1277(4)	-0.0919(4)	1	0.025(3)
O4	0.2614(7)	0	0	1	0.028(2)
O5	0.2246(4)	-0.2246(4)	0.1810(4)	1	0.021(2)
C1	0	0	0.1406(3)	0.99(2)	0.030(2)
C2	0	0	0.288(4)	0.07(2)	0.03(3)
C3	0	0	0.399(2)	0.32(4)	0.15(3)
C5	0	0	½	0.67(6)	0.040(12)
W1	0.151(1)	0.0757(5)	0.2118(6)	1	0.055(3)
W2	0.126(1)	0.251(2)	0.286(1)	0.36(2)	0.03(3)
W3	0.170(3)	0.115(2)	0.343(1)	0.19(1)	0.03(3)
W4	0.212(2)	0.424(5)	0.287(3)	0.17(2)	0.03(3)
	100 °C (SC-XRD)				
T1 (Si)	0.0004(2)	0.2323(1)	0.0698(1)	0.63	0.0141(9)
T1 (Al)	0.0004(2)	0.2323(1)	0.0698(1)	0.37	0.0141(9)
T2 (Si)	0.2408(2)	0	½	0.63	0.012(1)
T2 (Al)	0.2408(2)	0	½	0.37	0.012(1)
O1	0.0325(6)	0.349(1)	0.1080(3)	1	0.030(3)
O2	0.0914(5)	-0.0914(5)	0.0841(6)	1	0.029(3)
O3	0.1278(6)	-0.1278(6)	-0.0920(5)	1	0.035(4)
O4	0.2635(8)	0	0	1	0.029(3)
O5	0.2246(5)	-0.2246(5)	0.1783(5)	1	0.025(3)
C1	0	0	0.1397(4)	1	0.027(2)
C3	0	0	0.3957(1)	0.44(4)	0.14(2)
C5	0	0	½	1	0.01(5)
W1	0.149(1)	0.0748(8)	0.2116(8)	1	0.085(7)

W2	0.125(3)	0.251(6)	0.285(4)	0.18(3)	0.03 (3)
W3	0.130(3)	0.198(2)	0.3257(1)	0.20(1)	0.03(3)
W4	0.202(2)	0.405(5)	0.304(2)	0.22(1)	0.03(3)
	r*T* (rev) (SC-XRD)				
T1(Si)	0.0022(4)	0.2489(4)	0.0596(2)	0.517(11)	0.032(2)
T2(Si)	0.2481(2)	0	½	1	0.018(1)
O1	0.0159(8)	0.3528(8)	0.1099(3)	1	0.078(3)
O2	0.0974(7)	-0.0974(7)	0.0661(7)	0.473(8)	0.093(5)
O3	0.133	-0.133(5)	-0.0651(9)	0.34(2)	0.093(8)
O4	0.321(1)	0	0	1	0.080(4)
O5	0.2180(6)	-0.2180(6)	0.1656(7)		0.095(5)
T1B(Si)	0.0011(4)	0.2504(4)	0.2790(2)	0.402(4)	0.026(2)
OB1	0.5589(8)	0.1177(15)	0.0494(7)	0.86	0.087(7)
OB2	0.426(2)	0.2131(11)	0.062(1)	0.48(4)	0.071(10)
C1	0	0	0.114(2)	0.35(4)	0.180(3)
C3	0	0	0.287(1)	0.40(3)	0.089(9)
C5	0	0	½	0.22(3)	0.057(13)
C5B	0	0	0.4354	0.14(2)	0.011(2)
C6	0	0	0	0.37(4)	0.22(2)
C7	0.498(3)	0.249(2)	0.143(2)	0.29(2)	0.22(2)
W5	0.498(3)	0.249(2)	0.143(2)	0.43(4)	0.065 (3)
W6	0	0	0.382(2)	0.34(4)	0.081(15)
W7	-0.080(2)	0.080(2)	0.356(1)	0.47(4)	0.17(6)

	r*T (SR-XRPD)*				
	x/a	**y/b**	**z/c**	**F**	**Uiso**
T1	-0.0001(4)	0.2325(4)	0.0688(2)	1	0.0235(9)
T2	0.2416(4)	0	½	1	0.0235(9)
O1	0.0345(6)	0.3464(5)	0.1091(3)	1	0.044(2)
O2	0.0940(4)	-0.0940(4)	0.0827(5)	1	0.044(2)
O3	0.1267(5)	-0.1267(5)	-0.0929(6)	1	0.044(2)
O4	0.2674(7)	0	0	1	0.044(2)
O5	0.2183(4)	-0.2183(4)	0.1770(6)	1	0.044(2)
C1	0	0	0.1356(5)	0.88(1)	0.062(3)
C2	0	0	0.265(2)	0.17(9)	0.062(3)
C3	0	0	0.418(1)	0.37(1)	0.062(3)
C5	0	0	½	0.16(1)	0.062(3)
W1	0.158(1)	0.0792(5)	0.2132(7)	1.00(1)	0.106(4)
W2	0.122(6)	0.244(1)	0.2885(7)	0.99(1)	0.106(4)
W3	0.143(1)	0.0716(7)	0.3484(7)	0.79(1)	0.106(4)
W4	0.219(1)	0.438(3)	0.2846(9)	0.48(1)	0.106(4)
	266 °C (SR-XRPD)				
T1	0.0005(4)	0.2373(4)	0.0677(1)	1	0.0340(9)
T2	0.2453(4)	0	½	1	0.0340(9)
O1	0.0244(6)	0.3451(5)	0.1095(3)	1	0.050(2)
O2	0.0973(4)	-0.0973(4)	0.0779(5)	1	0.050(2)
O3	0.1283(5)	-0.1283(5)	-0.0888(6)	1	0.050(2)
O4	0.2735(7)	0	0	1	0.050(2)
O5	0.2201(3)	-0.2201(3)	0.1730(6)	1	0.050(2)
C1	0	0	0.1250(4)	0.92(1)	0.059(3)
C3	0	0	0.409(4)	0.14(2)	0.059(3)
C5	0	0	½	0.71(1)	0.059(3)
W1	0.134(1)	0.0670(8)	0.200(1)	0.70(1)	0.166(8)
W2	0.138(1)	0.276(2)	0.299(1)	0.61(1)	0.166(8)
W3	0.06(1)	0.029(5)	0.365(5)	0.06(2)	0.166(8)
W4	0.239(3)	0.479(5)	0.284(2)	0.35(1)	0.166(8)
	458 °C (SR-XRPD)				

T1	-0.002(1)	0.2406(9)	0.0613(3)	0.6	0.042(1)
T2	0.2544(6)	0	½	1	0.042(1)
O1	-0.013(1)	0.3136(8)	0.1167(4)	1	0.068(2)
O2	0.1035(8)	-0.1035(8)	0.063(2)	0.6	0.068(2)
O3	0.133(1)	-0.133(1)	-0.039(1)	0.6	0.068(2)
O4	0.2993(9)	0	0	1	0.068(2)
O5	0.2126(5)	-0.2126(5)	0.162(1)	1	0.068(2)
T1B	-0.0048(8)	0.2557(7)	0.2790(3)	0.4	0.042(1)
OB1	0.543(2)	0.087(4)	0.043(2)	0.4	0.068(2)
OB2	0.458(2)	0.229(1)	0.054(3)	0.4	0.068(2)
C1	0	0	0.124(3)	0.25(2)	0.086(8)
C3	0	0	0.233(9)	0.08(2)	0.086(8)
C5	0	0	½	0.13(3)	0.086(8)
C6	0	0	0	0.26(6)	0.086(8)
C8	0.252(3)	0.126(2)	0.147(2)	0.19(9)	0.086(8)
C9	0	0	0.049(3)	0.37(3)	0.086(8)

			SC-XRD				**SR-XRPD**		
			r*T*	**100°C**	**r*T* (rev)**		**r*T***	**266°C**	**458°C**
T1-	**O1**		1.657(9)	1.65(1)	1.723(8)		1.637(6)	1.618(6)	1.650(8)
	O2		1.686(4)	1.682(6)	1.690(7)		1.670(4)	1.653(4)	1.610(9)
	O3		1.650(4)	1.658(5)	1.633(3)		1.667(5)	1.662(5)	1.631(9)
	O4		1.653(3)	1.644(4)	1.686(9)		1.642(4)	1.643(5)	1.621(9)
	Average		*1,661*	*1,659*	*1,683*		*1,654*	*1.644*	*1,627*
T1-	**T1B-**				*1.904(6)*				*1.76(1)*
T2-	**O1**	(x2)	1.634(7)	1.629(9)	1.588(6)		1.618(6)	1.623(5)	1.694(8)
	O5	(x2)	1.658(3)	1.653(4)	1.607(2)		1.638(3)	1.642(3)	1.635(5)
	Average		*1,646*	*1,639*	*1,598*		*1,628*	*1.632*	*1,664*
T1B-	**O1**				1.752(8)				1.744(7)
	O4				1.722(7)				1.767(6)
	OB1				1.645(6)				1.719(7)
	OB2				1.629(5)				1.706(8)
	Average				*1,687*				*1,734*
C1-	**O2**	(x3)	2.443(10)	2.47(2)	2.44(3)		2.486(6)	2.481(5)	2.71(3)
	O3	(x3)			3.17(9)		3.091(4)	3.055(3)	
	W1	(x3)	2.390(13)	2.38(1)			2.576(8)	2.33(2)	
	W7				2.01(10)				
C2-	**W1**	(x3)	2.47(7)				2.20(3)		
	W2	(x3)	2.92(3)				2.857(7)		
	W3	(x3)	2.38(6)				2.51(3)		
C3-	**O5**	(x3)	3.21(4)	3.28(3)			3.12(1)		
	W3	(x3)	2.38(4)	2.82(4)			2.31(2)	1.22(10)	
	W4	(x3)	2.85(6)	3.12(5)			2.780(7)	2.24(6)	
	W5				2.24(6)				
	W6	(x3)			2.41(4)				
	W7				2.05(7)				

	OB1	(x3)			2.402(17)				3.02(12)
	OB2	(x3)			2.70(3)				2.56(12)
C5-	**O5**	(x6)	2.548(9)	2.539(7)	2.568(12)		2.6759(1)	2.5966(6)	2.6859(1)
	W5	(x2)			2.75(5)				
C5B	**O5**	(x3)			2.968(14)				
	O5	(x3)			2.993(14)				
	W6	(x3)			2.56(4)				
C6-	**O2**	(x6)			2.664(14)				2.7341(1)
	O3	(x6)			3.331(9)				3.0693(2)
C7-	**O1**	(x2)			3.08(2)				
	O3				3.13(6)				
	OB1				3.10(4)				
	OB2				2.07 (4)				
	W7				1.89(4)				
C8-	**O1**	(x2)							2.20(2)
	O1								2.71(3)
	O3								2.56(4)
	OB2								3.17(4)
	OB2								3.18(4)
C9-	**O2**	(x3)							2.32(1)
	O3	(x3)							2.945(6)
W1-	**C1**		2.39(1)	2.38(2)			2.55(1)	2.328(23)	
	C2		2.47(7)				2.20(3)		
	O3						2.95(1)	2.945(24)	
	O3						3.01(1)		
	W1	(x2)					3.18(2)	2.658(30)	
	W2	(x2)					3.02(2)		
	W3						3.10(2)		

W2-	**C2**		2.92(3)				2.87(1)		
	O1	(x2)					3.08(1)	2.967(22)	
	O4	(x2)						3.166(9)	
	W1	(x2)					3.02(2)		
	W2						2.91(3)	2.05(5)	
	W3			1.18(7)			2.82(1)		
	W4			1.77(9)			2.25(3)	2.34(6)	
	W4						2.15(1)	2.180(13)	
W3-	**C2**		2.38(6)				2.51(2)		
	C3		2.38(4)	2.82(4)			2.30(2)	1.22(10)	
	W1						3.10(2)		
	W2	(x2)					2.82(1)		
	W3	(x2)	0.82(5)	0.83(4)			2.87(3)	1.16(19)	
	W4	(x2)					2.44(2)	2.85(14)	
	W4	(x2)		1.20(5)				1.95(6)	
W4-	**C3**		2.85(5)	3.12(5)			2.77(3)	2.24(6)	
	O1	(x2)					2.79(1)	2.96(5)	
	O5						2.45(2)	2.61(6)	
	W2						2.25(3)	2.34(6)	
	W2			1.77(9)			2.15(1)	2.18(1)	
	W3	(x2)					2.44(2)	2.85(14)	
	W3	(x2)		1.20(6)				1.95(6)	
W5	**C3**				2.24(5)				
	C5	(x2)			2.75(4)				
W6-	**O4**	(x2)			2.98(1)				
	OB1	(x2)			2.74(1)				
	OB2				2.18(1)				
W7-	**OB1**	(x3)			3.11(1)				
	OB2	(x3)			3.17(1)				

	D6R							**6mR**		**8mR**	
T (°C)	**O1-O4-O1**	**O1-O1**	**O4-O4**	**O3-O2**	**O3-O2-O3**	**O2-O3-O2**		**O5-O5**		**O5-O5**	**O4-O4**
28	**143.93**	5.06	7.16	5.12	147.5	90.5		5.35		7.51	6.22
52	**142.55**	5.02	7.14	5.09	148.04	88.6		5.32		7.55	6.35
69	**140.65**	5	7.06	5.01	150.23	86.24		5.31		7.62	6.35
87	**141.02**	4.99	7.06	4.91	152.12	85.3		5.3		7.52	6.34
105	**140.32**	4.99	7.06	4.98	150.6	86.51		5.24		7.6	6.34
123	**141.14**	5.01	7.07	5	151.21	86.37		5.24		7.59	6.39
141	**139.73**	5	7.03	5.01	150.2	87.03		5.31		7.65	6.33
158	**142.46**	5.04	7.12	5	148.53	88.96		5.18		7.6	6.31
176	**142.39**	5.02	7.09	5	148.5	88.95		5.11		7.63	6.23
194	**140.55**	5.03	7.04	5.05	146.7	90.8		5.28		7.66	6.26
213	**142**	5.03	7.07	5.1	146.5	90.92		5.27		7.69	6.2
230	**143.02**	5.06	7.1	5.16	146.35	91.26		5.24		7.74	6.16
248	**144.52**	5.08	7.15	5.18	145.41	91.56		5.24		7.77	6.09
266	**145.68**	5.1	7.21	5.18	145.08	91.67		5.21		7.82	6
458	*169.01*	*5.51*	*7.64*	*5.26*	*137.24*	*92.98*		*5.34*		*8.33*	*5.12*

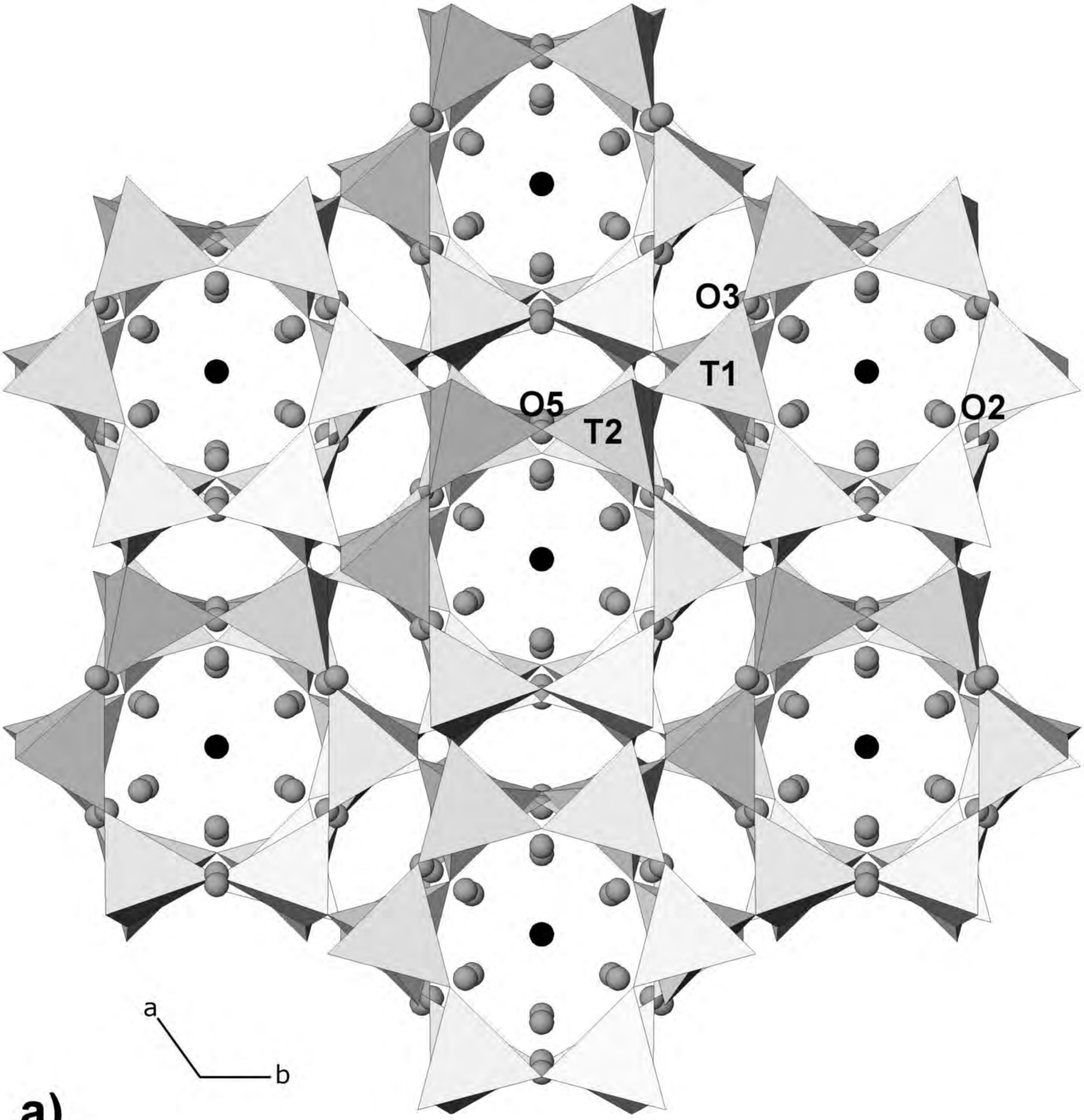

figure 1a

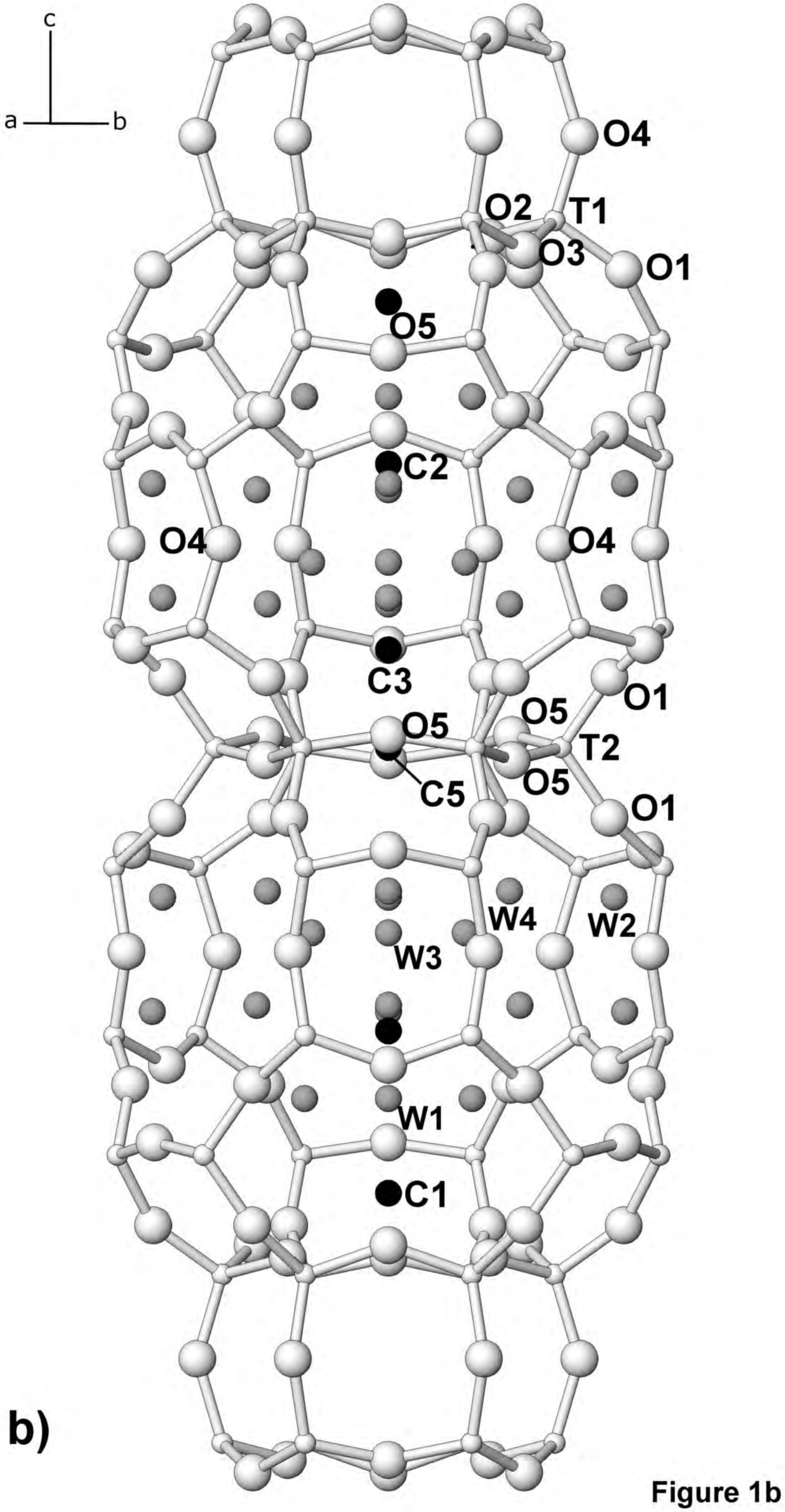
c
a
b
O4
O2
T1
O3
O1
O5
C2
O4
O4
C3
O1
O5
O5
T2
O5
C5
O5
O1
W4
W2
W3
W1
C1
b)

Figure 1b

Figure 2

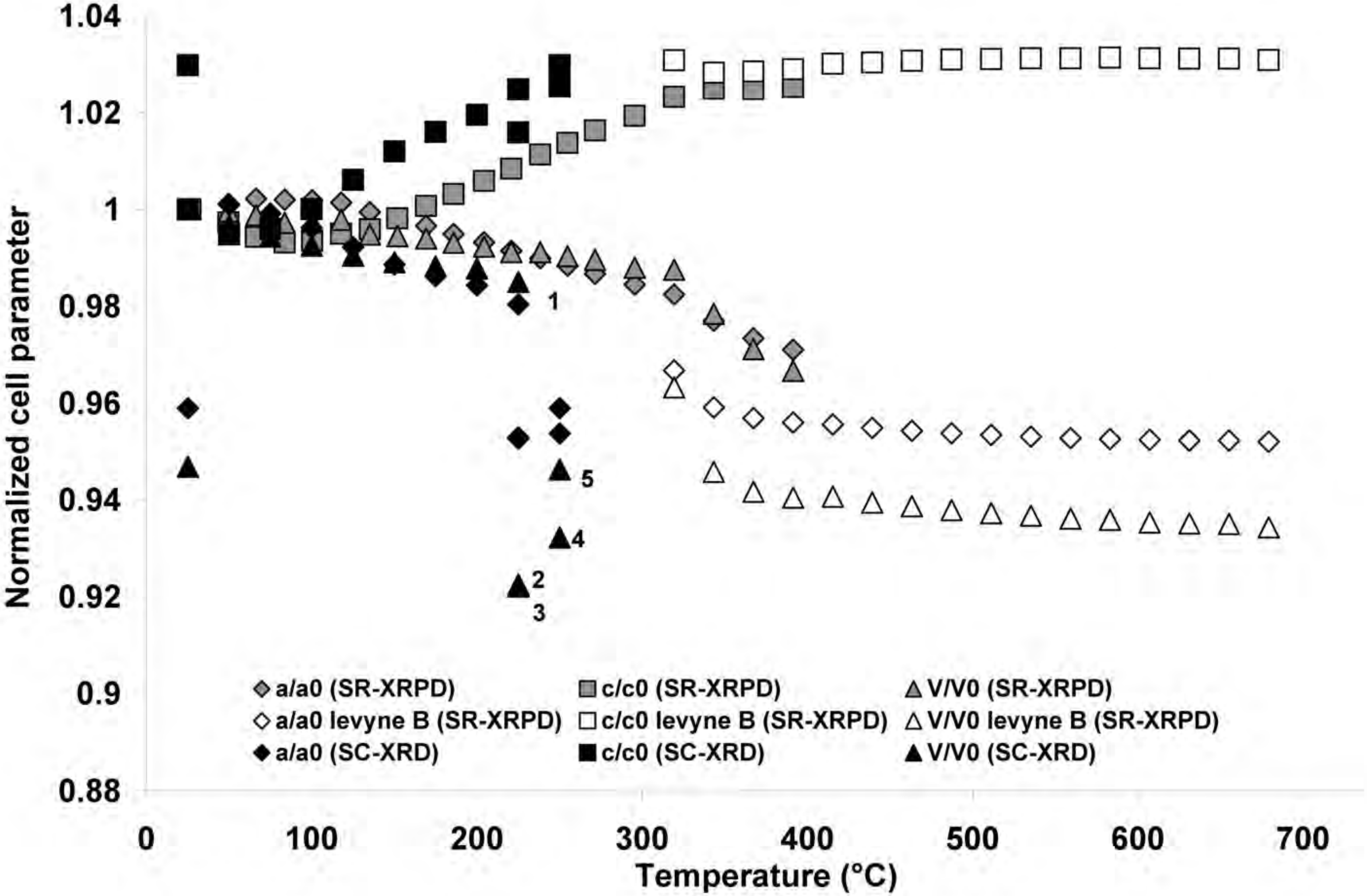
1.04
1.02
1
0.98
0.96
0.94
0.92
0.9
0.88
Normalized cell parameter
0
100
200
300
400
500
600
700
Temperature (°C)
1
2
3
4
5
◆ a/a0 (SR-XRPD)
■ c/c0 (SR-XRPD)
▲ V/V0 (SR-XRPD)
◇ a/a0 levyne B (SR-XRPD)
□ c/c0 levyne B (SR-XRPD)
△ V/V0 levyne B (SR-XRPD)
◆ a/a0 (SC-XRD)
■ c/c0 (SC-XRD)
▲ V/V0 (SC-XRD)

figure 3

Figure 4

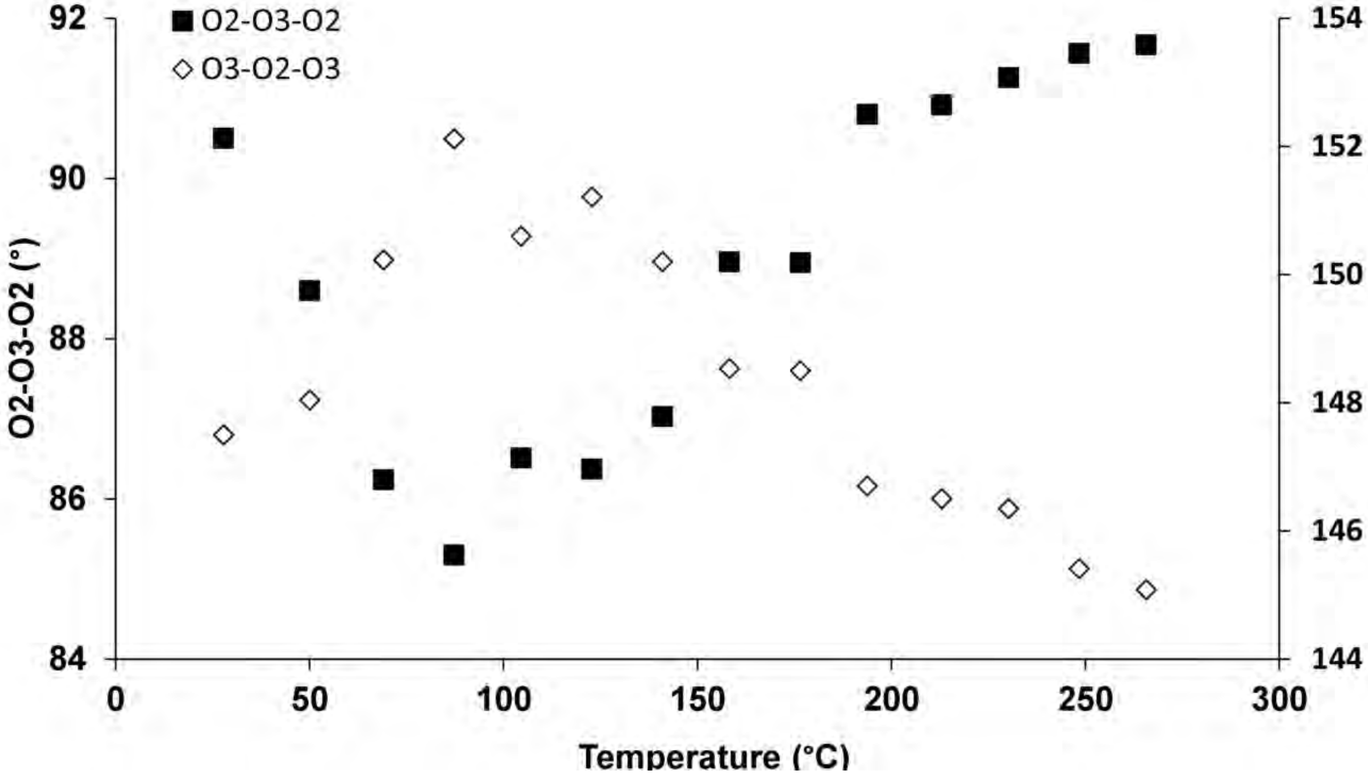
■ O2-O3-O2
◇ O3-O2-O3
O2-O3-O2 (°)
O3-O2-O3 (°)
Temperature (°C)
92
90
88
86
84
154
152
150
148
146
144
0
50
100
150
200
250
300

Figure 5

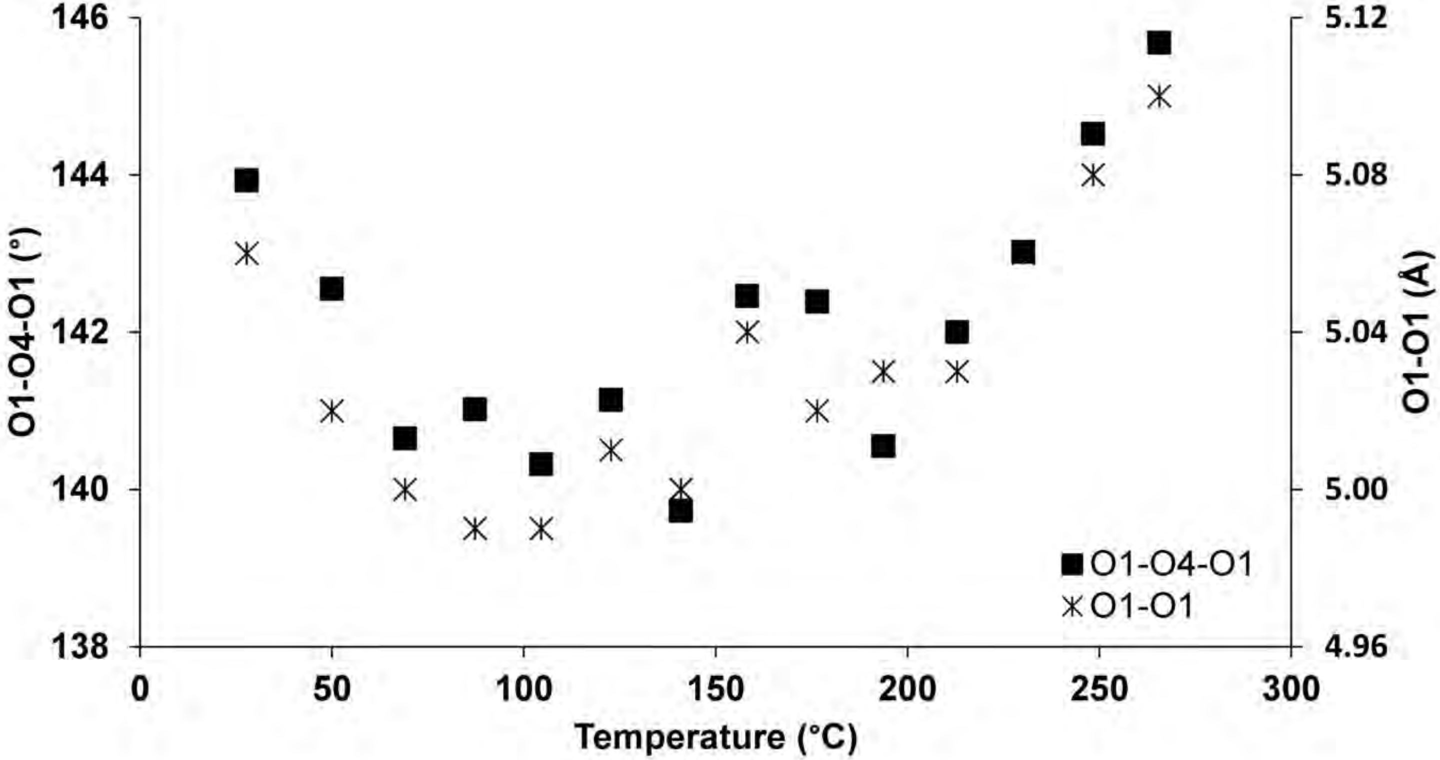
146
144
142
140
138
O1-O4-O1 (°)
5.12
5.08
5.04
5.00
4.96
O1-O1 (Å)
0
50
100
150
200
250
300
Temperature (°C)
■ O1-O4-O1
✳ O1-O1

Figure 6

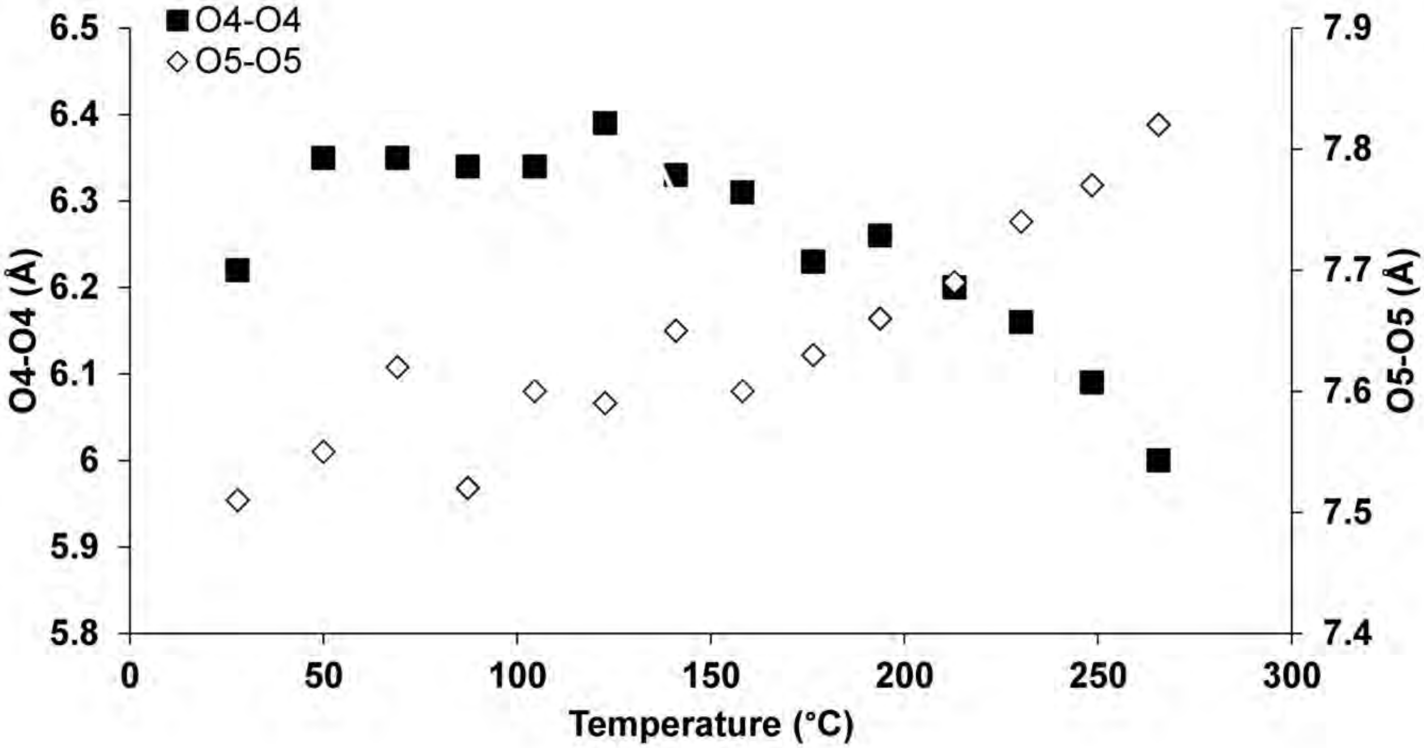
■ O4-O4
◇ O5-O5
O4-O4 (Å)
O5-O5 (Å)
Temperature (°C)
6.5
6.4
6.3
6.2
6.1
6
5.9
5.8
7.9
7.8
7.7
7.6
7.5
7.4
0
50
100
150
200
250
300

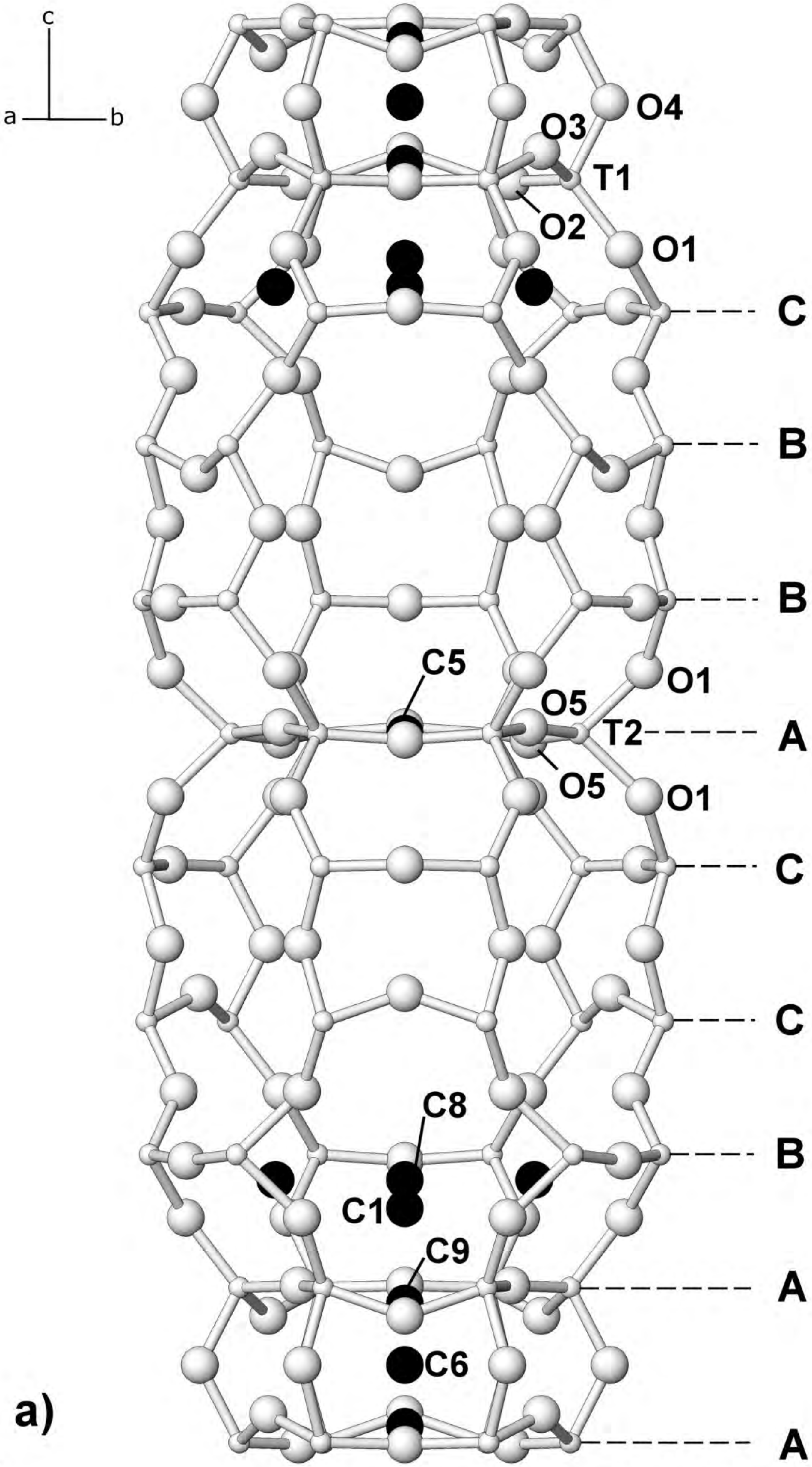

Figure 7a

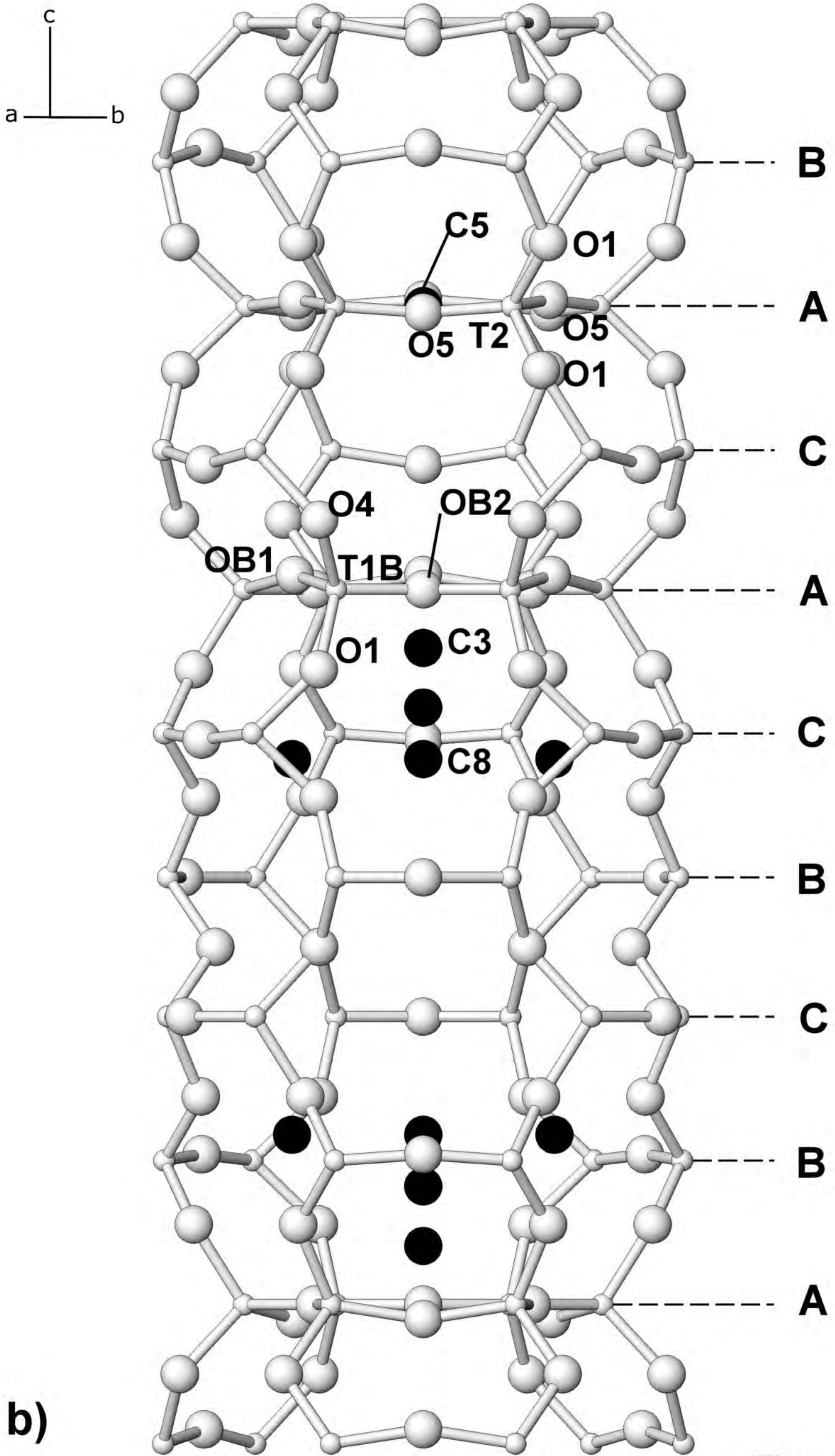

Figure 7b

Figure 8

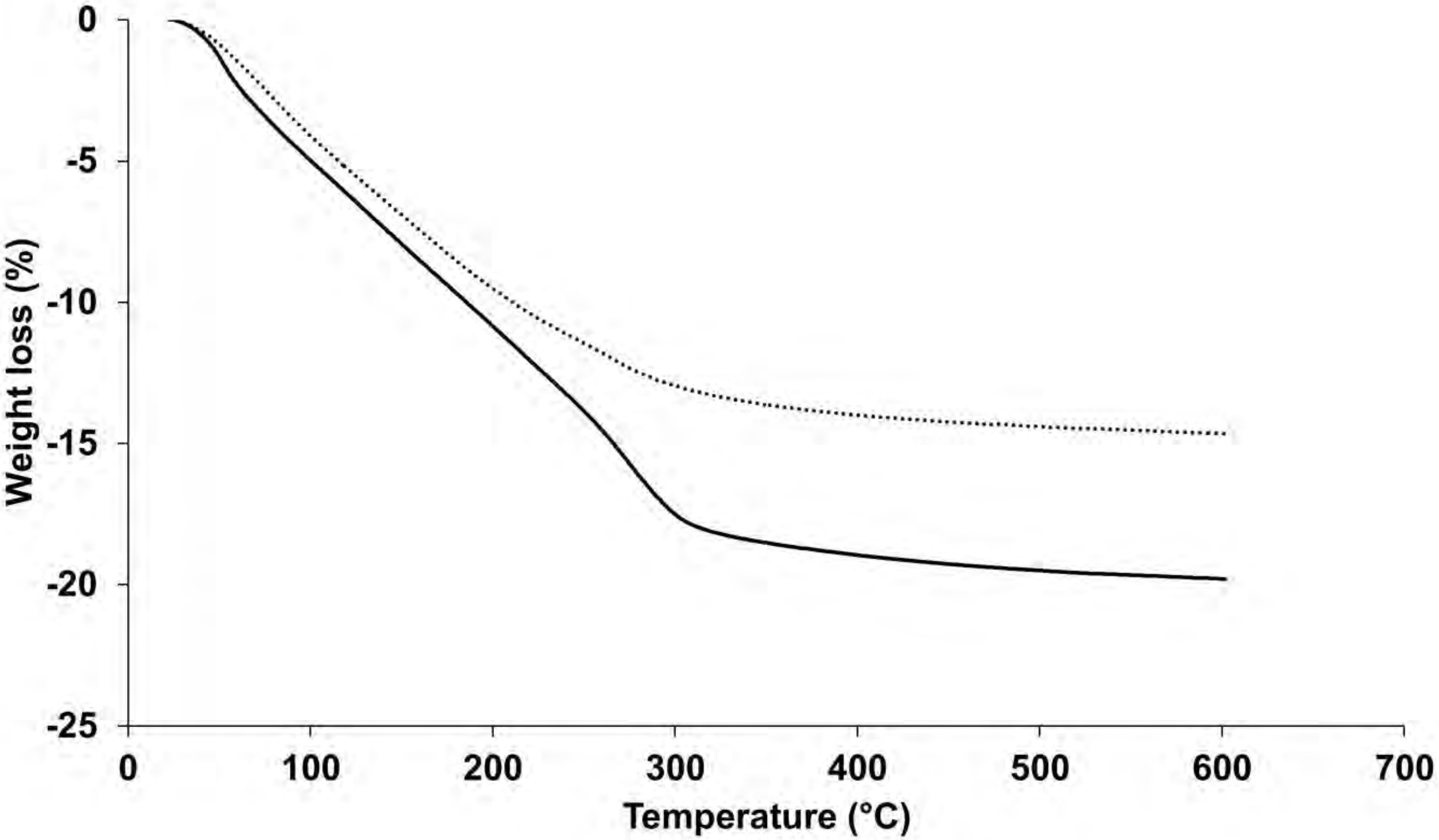
0
-5
-10
-15
-20
-25
Weight loss (%)
0
100
200
300
400
500
600
700
Temperature (°C)

Figure 9a

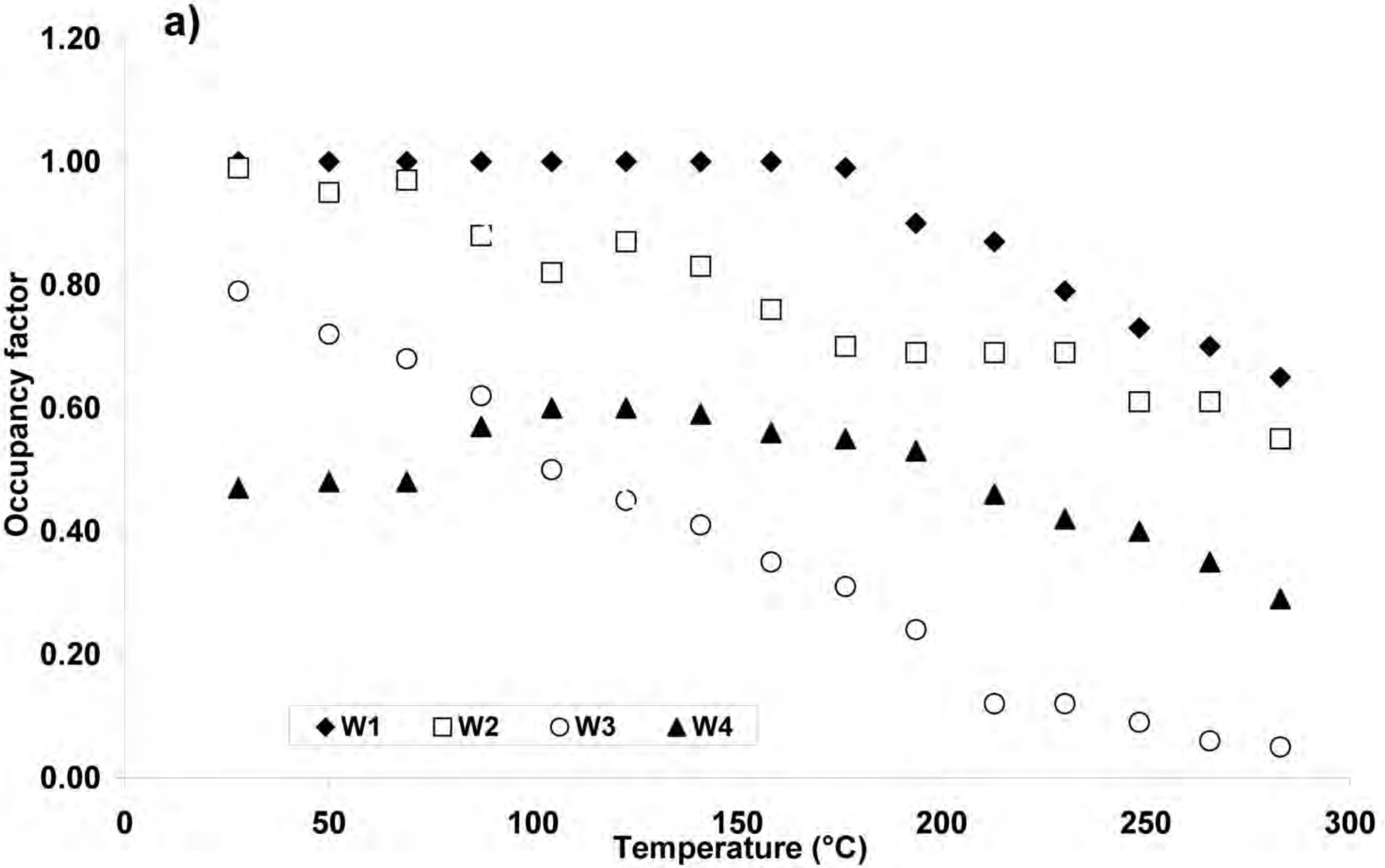
a)
Occupancy factor
1.20
1.00
0.80
0.60
0.40
0.20
0.00
0
50
100
150
200
250
300
Temperature (°C)
◆ W1
□ W2
○ W3
▲ W4

Figure 9b

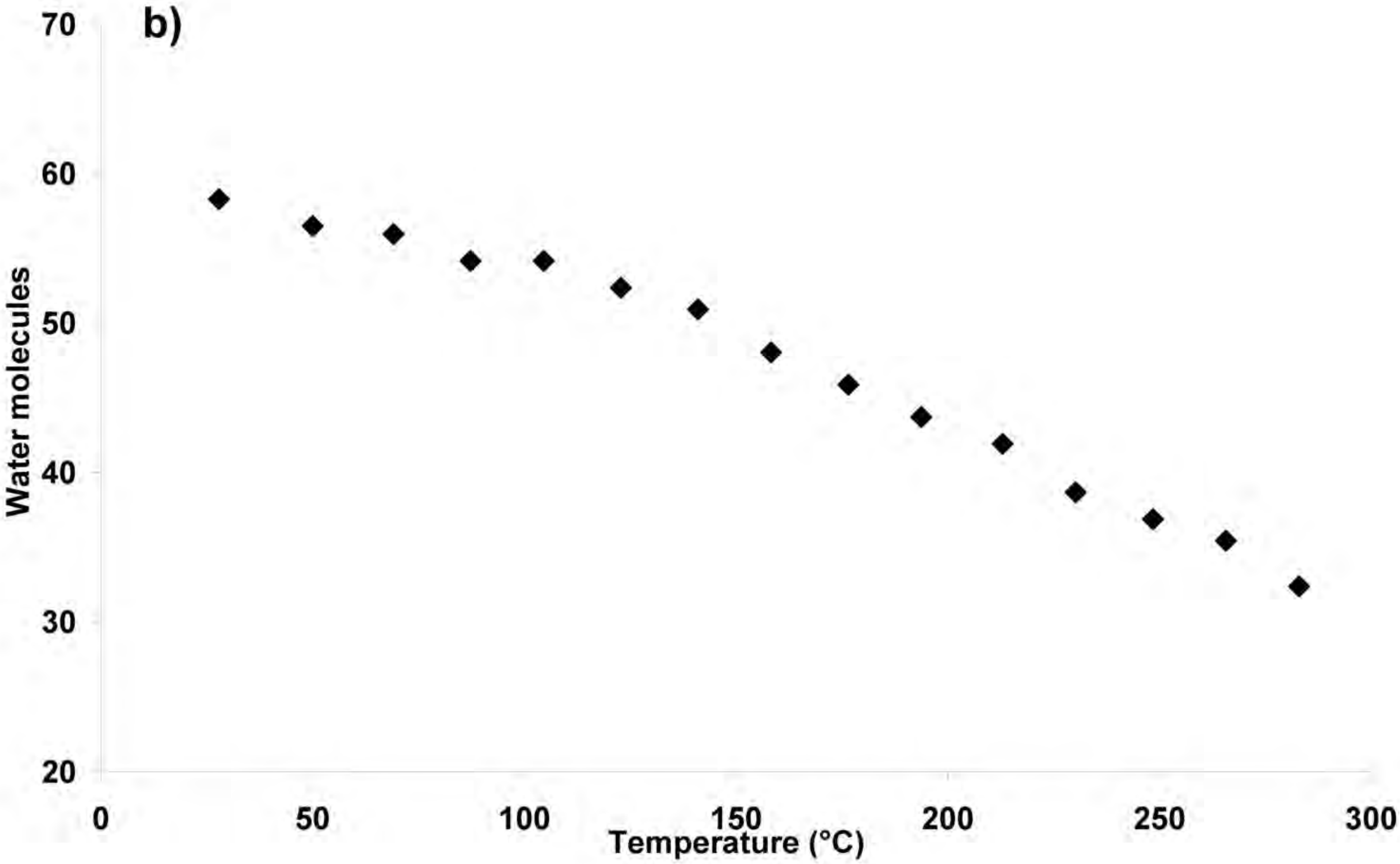
b)
Water molecules
70
60
50
40
30
20
0
50
100
150
200
250
300
Temperature (°C)

Figure 10

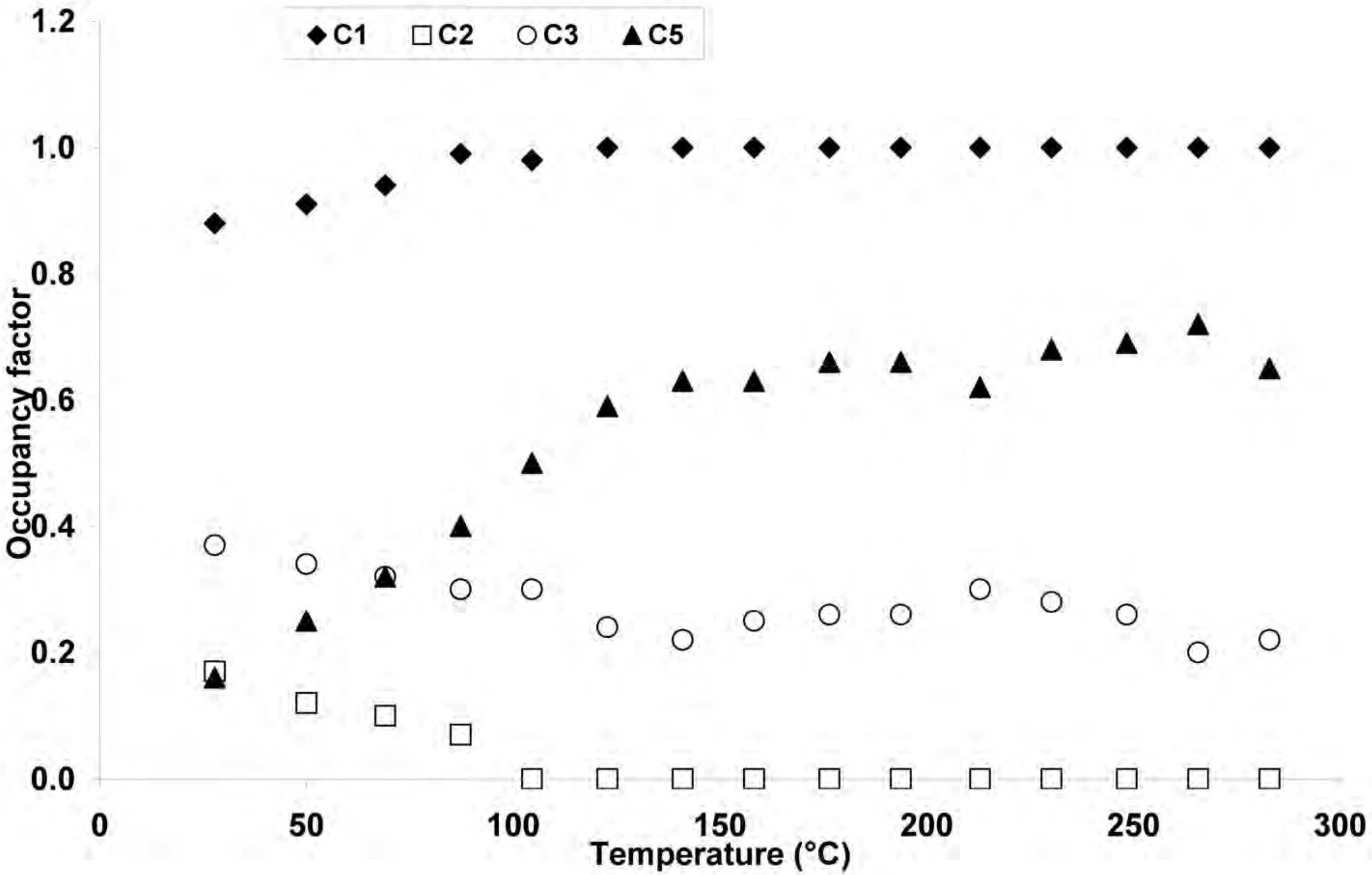
◆ C1
□ C2
○ C3
▲ C5
Occupancy factor
1.2
1.0
0.8
0.6
0.4
0.2
0.0
0
50
100
150
200
250
300
Temperature (°C)